Cloud Computing Based Hydrodynamic Model HYDROTAM3D

Sea and Aquatic Sciences Application and Research Center
Gazi University
06570 Ankara Turkey
e-mail: lalebal@gazi.edu.tr

ABSTRACT

HYDROTAM 3D is a Geographic Information Systems(GIS) based three-dimensional, baroclinic numerical model developed to simulate the hydrodynamic and transport processes in coastal waters. As the infrastructure it is based on cloud computing. In its interface all functions of the MS Silverlight framework are available to the user in a menu driven graphical user interface. The numerical model consists of wind and wave climate, wave propagation, hydrodynamic, transport, turbulence and water quality model components. In the wind and wave climate model, long term and extreme statistics methods are used to determine wind and wave roses and dominant wave properties based on the database of hourly measured wind data of all the coastal Turkish Meteorological Stations which are available between the years of 1970-2018. The locations of all the coastal Turkish Meteorological Stations are shown on the map of Turkey based on GIS. Additionally, in the database, six hourly numerical weather and wave predictions of ECMWF(European Centre for Medium Range Weather Forecast) operational and ERA archive exist at every 0.1 degree horizontal grid spacing covering all of Turkish coastal waters between 2000-2018. In the wave propagation submodel, mild slope equations are solved. In the hydrodynamic model component, the 3D Navier–Stokes equations are solved with the Boussinesq approximation. The transport model component consists of the pollutant, water temperature and salinity, longshore sediment and suspended sediment transport models. In the turbulence model, a two-equation k–ε formulation is solved to calculate the kinetic energy of the turbulence and its rate of dissipation. In the water quality model component, biochemical cycles simulated are the cycles of nitrogen, phosphorus, and oxygen. Organisms simulated in the model are the low tropic levels in aquatic environments.

Keywords: Hydrodynamic, transport, numerical model, cloud computing, environmental software, HYDROTAM 3D

1. Introduction

Wind, waves and currents are basic parameters that shape the coasts. Understanding the coastal process is vital issue to design and manage the coasts. Design and management of coasts are very complicated therefore they require integrated approach. With the models, physical, chemical and biological behaviours can be simulated quickly and economically. There are different coastal models such as MIKE 21 (http://www.mikepoweredbydhi.com/products/mike-21, Lawen et al., 2012,), Delft 3d (http://www.deltaressystems.com/hydro/product/621497/delft3d-suite, Rijn et al., 2004), Flow 3D (http://www.flow3d.com/), SWAN (http://www.swan.tudelft.nl/, Booij et al., 1996, 1999, Ris et al., 1999), MOHID (http://www.mohid.com/, Braunschweig et al., 2004, Neves, 2007), CORMIX (http://www.cormix.info/, Palomar et al., 2012a, 2012b, Lawen et al., 2012) etc. They focus on hydrodynamic, wind and wave climate, wave, sediment, water quality modeling, which describe the coastal prosesses. They can be used as forecast and early warning tools. At first, the wind and wave climate of a coastal region should be determined to understand study field. Hydrodynamic modelling

is main part of mostly coastal tasks. Besides it is important in itself, it give inputs for sediment transport, water quality or ecological system models. Environmental impacts, coastal and ocenographic circulations, hydrodynamics of coastal regions like bays, lagoons, the distrubution of saline or brine waters can be simulated with hydrodynamic modeling tools. Number of activities in coastal engineering is based on wave modeling. Wave conditions in an coastal area should be known for the design, construction and installations of coastal structures, renewable energy devices at the sea. Wave propagations, transformations, dissipations and transmissions through and reflections against obstacles are simulated with wave models. To determine erosion, deposition, establishment and conservation of beaches, dredging operations in harbors, sediment tranport should be simulated. Complex ecosystem behaviour, like eutrophication, heavy metals of the system should be analysed using water quality modeling. Since HYDROTAM-3D (hydrotam.com)uses cloud computing, it provides a wide range of users with distributed access to scalable, virtualized hardware and/or software infra-structure over the internet. It has wind and wave climate, wave propagation, hydrodynamic, transport and turbulence, water quality model components.

2. Cloud Computing

In general, cloud computing is a distributed computing paradigm that focuses on providing a wide range of users with distributed access to scalable, virtualized hardware and/or software infra-structure over the internet. Many definitions have been offered for this term (Strowd and Lewis, 2010). Cloud computing is defined as a large-scale distributed computing paradigm that is driven by economies of scale, in which a pool of abstracted, virtualized, dynamically-scalable, managed computing power, storage, platforms, and services are delivered on demand to external customers over the internet (Foster, 2008). Cloud computing is a new generation of computing that uses distant servers to provide services and storage accessed over the Internet, often on a consumption-based model. Typical cloud computing providers deliver applications online that are accessed from a Web browser while user data is stored on remote servers. In cloud computing, those servers are usually owned and maintained by a third-party provider on a consolidated basis in a remote data center. Cloud computing implementations can be characterized in two ways: by the capabilities they provide and by who can access their resources. Based on capabilities, there are basically three types of cloud computing implementations, namely Infrastructure as a Service (IaaS)**,** Platform as a Service (PaaS) and Software as a Service (SaaS) (Balas et al., 2011).

Infrastructure as a Service (IaaS)

This is mainly computational infrastructure available over the internet, such as compute cycles and storage, which can be utilized in the same way as internally owned resources. IaaS providers en-force minimal restrictions on their users to allow them maximum control and configuration of the resources. These resources typically provide a variety of interfaces to facilitate interaction, and there are usually additional services provided, such as query services for storage resources

Platform as a Service (PaaS)

PaaS refers to application development platforms (hardware and software components) that enable users to leverage the resources of established organizations to create and host applications of a larger scale than an individual or a small organization would be

able to handle. Services include, but are not limited to, software installation and configuration, resource scaling, and platform maintenance and upgrading. In order to enable these services, the provider places restrictions on the user by specifying various aspects of the platform, such as the programming languages supported, data storage mechanisms, and resource monitoring capabilities. In this model, user organizations use resources from the cloud and deploy their applications in the cloud as well. From the user's perspective, these providers offer significant functionality out-of-the-box.

Software as a Service (SaaS)

SaaS focuses on providing users with business-specific capabilities (hardware and software applications). In general, SaaS is a model of software deployment in which a provider licenses an application to user organizations for use as a service on demand. HYDROTAM 3D is a model of IaaS. IaaS is the base layer of the cloud stack. It serves as a foundation for the other two layers, for their execution (Fig.1). The drivers for cloud computing adoption of HYDROTAM 3D are listed in Table 1 [Strowd and Lewis, 2010]. HYDROTAM 3D is also a good example of the Modeling as a Service (MaaS) initiative. Similar to SaaS, MaaS would allow the deployment and on-demand execution of modeling and model-driven services over the Internet.Cloud computing structure of the model HYDROTAM 3D is presented in Fig.2.

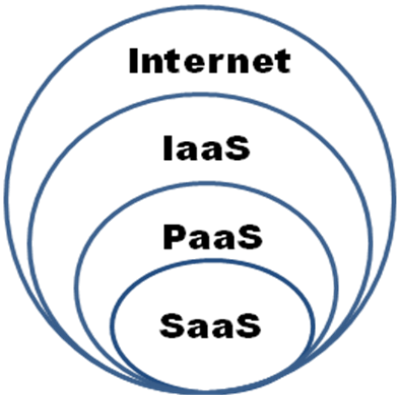

Fig. 1: Types of cloud computing implementations (Balas et al., 2011).

Table 1: Drivers for Cloud Computing

Driver	***Description***
Availability	Users have the ability to access their resources at any time through a standard internet connection.
Collaboration	Users are starting to see the cloud as a way to work simultaneously on common data and information.
Elasticity	The provider transparently manages a user's resource utilization based on dynamically changing needs.
Lower Infrastructure Costs	The pay-per-usage model allows an organization to pay only for the resources it needs, with basically no investment in the physical resources available in the cloud. There are also no in-frastructure maintenance or upgrade costs.
Mobility	Users have the ability to access data and applications from around the globe.
Risk Reduction	Organizations can use the cloud to test ideas and concepts before making major investments in technology.
Scalability	Users have access to a large amount of resources that scale based on user demand.
Virtualization	Each user has a single view of the available resources, independently of how they are arranged in terms of physical devices. Therefore, there is potential from a provider perspective to serve a greater number of users with fewer physical resources.

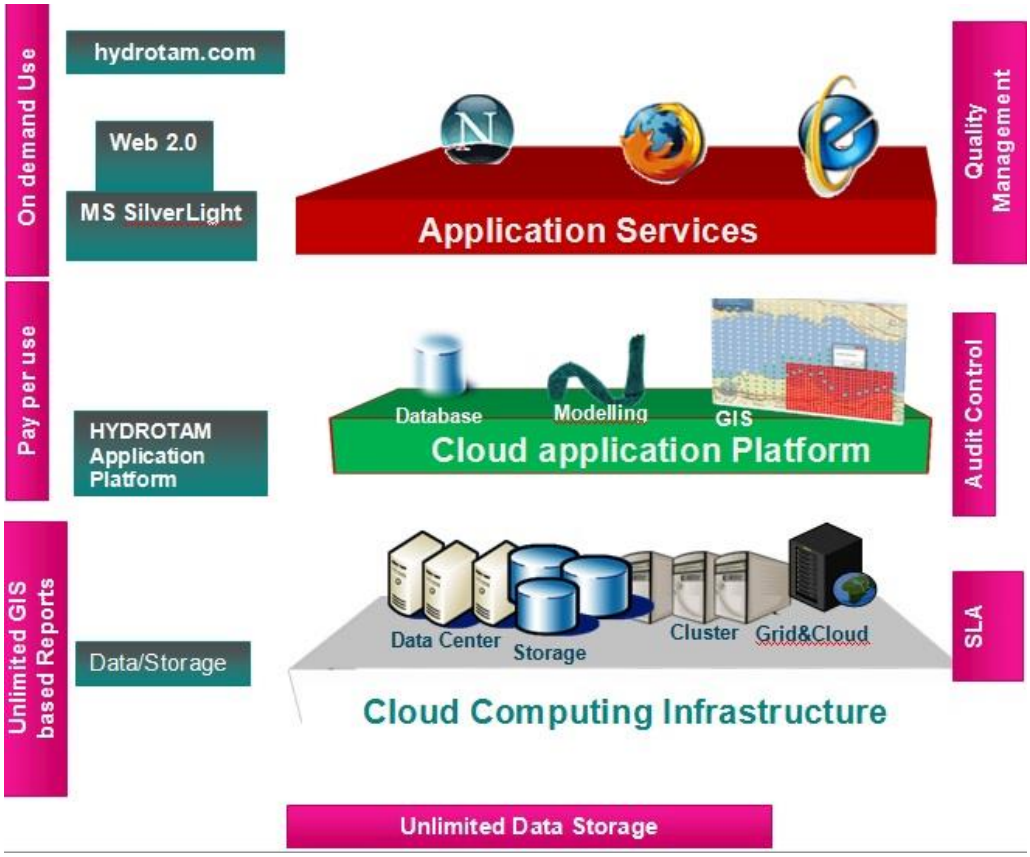

Fig. 2: HYDROTAM 3D Cloud Computing Structure (Balas et al., 2011)

3. HYDROTAM 3D Application Services

Enclosed or semi-enclosed coastal areas have limited water exchange. Therefore, to understand water circulations and transport processes is a delicate matter. Since field measurements are usually costly and sometimes impossible due to physical inabilities, application of numerical models becomes more and more important in the simulations of coastal water processes. Use of three-dimensional models is unavoidable in all cases where the influence of density distribution, or the vertical velocity variations cannot be neglected and in the simulation of wind induced circulation. HYDROTAM 3D predictions have been verified by using several experimental and analytical results published in the literature since 1990 and its successful use for a variety of real life cases along Turkish coastline has been demonstrated (Balas, 2001, 2004; Balas and Özhan, 2000, 2001, 2002, 2003; Balas and İnan 2005, 2010; Balas et al, 2011, 2012; Numanoglu Genc et al. 2013; Yıldız et al. 2005).

HYDROTAM 3D is a Geographic Information Systems (GIS) integrated three-dimensional baroclinic numerical model that has been developed to simulate the hydrodynamic and transport processes in coastal waters. The infrastructure of the program is based on cloud computing technology. GIS platform facilitates the time consuming task of preparation of data input and output. In its interface all functions of the MS Silverlight framework are available to the user in a menu driven graphical user interface. The numerical model consists of hydrodynamic, transport, turbulence and wave propagation model components. In the hydrodynamic model component, the 3D Navier–Stokes equations are solved with the Boussinesq approximation. The transport model component

consists of the pollutant transport, water temperature and salinity transport and suspended sediment transport models. In the turbulence model, a two-equation k–e formulation is solved to calculate the kinetic energy of the turbulence and its rate of dissipation, which provides the variable vertical turbulent eddy viscosity. In wave propagation component, mild slope equations are solved. Model involves electronic atlas of wind climate, wave climate and current climate of Turkish coastline. The basic model properties of HYDROTAM 3D are summarized as: It is three dimensional numerical model applicable to irregular bottom topography. It includes change of all variables with respect to time. The model can be run for any timeframe. It does not require any hardware, software investment and system management since it is based on cloud computing technology. It is fast as it can use multi-processor environment. The model input and output are Geographic Information System (GIS) based. It uses global coordinate system. Turkish coastline and most of the Turkish Bay bathymetries are provided on GIS mapping. Wind roses based on 20 years of meteorological data (1970-2018) are also provided for all the Turkish Meteorological Stations. According to the selected bay location that the user wants to investigate the current pattern or the transport mechanisms, nearest Meteorological Stations wind roses are served to the user. Finite volume and finite difference method is used calculations. It is a baroclinic model, i.e. it can handle water temperature, salinity and density variations as well as baratropic pressure gradients. Pointwise density, water temperature and salinity can be defined to the model. It includes Corriolis factor effect in the computations. Model can form graphically monthly, seasonal and yearly wind and wave roses. Database includes 44 years of hourly wind data from the meteorological stations (MS) of Turkish Coasts. It performs long-term and extreme analyses of the wind data for the selected Turkish coastal MS. Additionally, in the database, numerical weather prediction model six hourly analyzed wind data of ECMWF(European Centre for Medium Range Weather Forecast) exists at every 0.1 degree horizontal grid spacing covering all of Turkish coastal waters between years 2000-2018. Wind climate, also, is obtained based on ECMWF operational or ERA archive wind data (WIND CLIMATE SUB MODEL). If needed, locational wind data may be loaded by the user. Bathymetric data can be also loaded to the system by the user. Model allows multi-point selection to report the model results graphically and timewise. Three dimensional modeling of wind, tidal or density stratification based currents, change in water surface elevation and storm surge is included (HYDRODYNAMIC SUB MODEL). It includes three dimensional k-ε model (TURBULENCE SUB MODEL). Three dimensional modeling of diffusion and advection of a pollutant or suspended sediment mixed into coastal waters is solved. In case of sea outfall discharge (bacterial or heated water) nearfield and farfield dilution is modeled (POLLUTANT TRANSPORT SUB MODEL). Model predicts deep water significant wave heights and periods based on CEM Method. Also, predicted significant deep water heights and periods at every 0.1 degree horizontal grid spacing and 6 hour time intervals covering all of Turkish coastal waters between years 2000-2018 by ECMWF using the third generation wave model WAM (ERA-interim data), exists in the database. Long-term wave statistics and extreme wave statistics have been performed based on wave data (WAVE CLIMATE SUB MODEL).It simulates the transformation of waves from the deep water to the shallow waters using mild slope equations. It considers the effects of shoaling, refraction, diffraction, bottom friction, breaking and wave run-up. It simulates wave induced currents in the surf zone (WAVE PROPAGATION SUB MODEL). It simulates the sediment transportation due to breaking waves (LONGSHORE SEDIMENT TRANSPORT SUB MODEL).

It is applicable to coastal estuaries, lagoons and lakes. In this work, wind climate, wave climate, hydrodynamic, turbulence and pollutant transport, wave propgation, longshore sediment transport, water quality sub models of HYDROTAM 3D are presented. HYDROTAM 3D application services are given in Fig.3 (http://www.hydrotam.com). The model predictions were verified by using several experimental and analytical results published in the literature and its successful use for a variety of real life cases was demonstrated (Balas, 2001; Balas and Özhan, 2002).

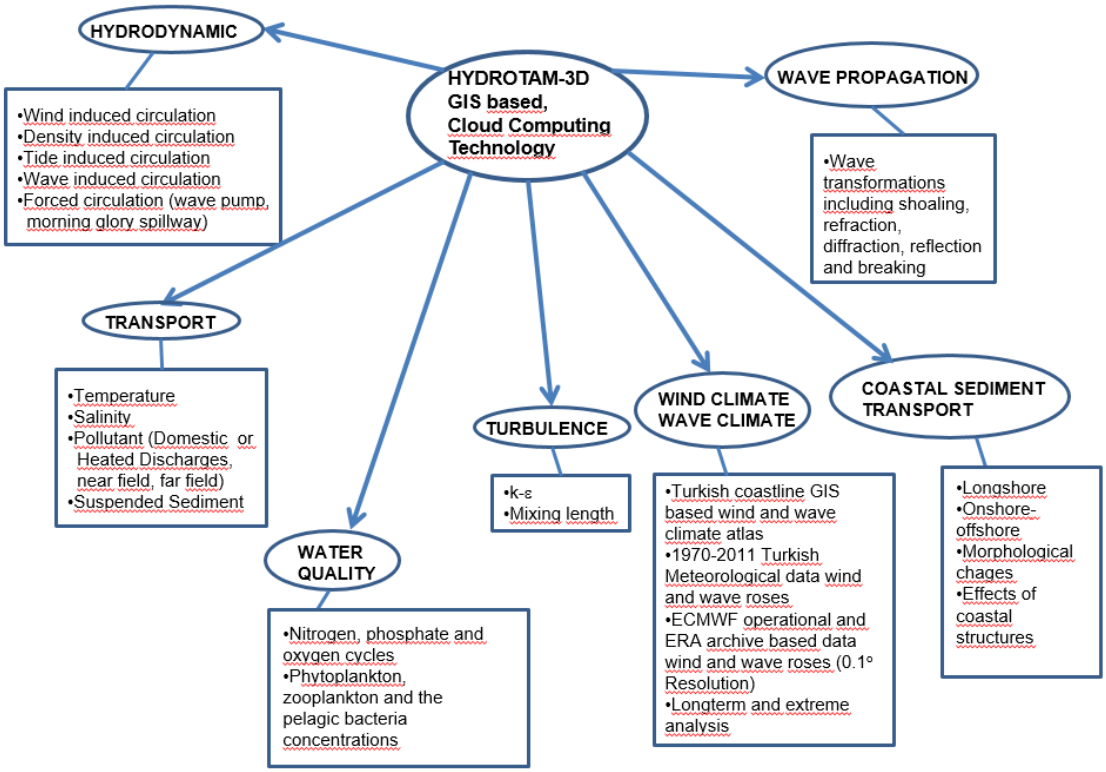

Fig.3: HYDROTAM 3D Application Services

4. Hydrodynamic and Turbulence Sub Models:

Water flows can be generally classified into two major categories, namely the small scale flow and the large scale water flow. Flows over trenches in the sea bottom, flows around fixed or floating structures, flows near intake or discharge points of a lake or a reservoir and flows in a river bend are examples of flows in the first category. The common characteristic of such flows is that the length scales of the flow field in the horizontal and vertical directions are of the same magnitude. As examples of flow in the second category, flows in the coastal water bodies such as lakes, estuaries, lagoons or bays, where the horizontal length scale is much larger than the vertical one, can be listed. There are various forces which drive the large-scale flows. Some are external and some are due to the nature of the fluid itself. Forces such as the gravity, the tide producing forces due to the sun and the moon, the stress of the wind acting on the sea surface, are external. The pressure gradient force and the viscous stresses are typical internal forces. There is in addition, the Coriolis force which is due to the rotation of the earth. This fictitious force performs no work. The concept of a Coriolis force simplifies mathematical descriptions of nearly all the large scale fluid phenomena of the earth. It is a means of accounting for the behavior of

particles moving in an inertial system but observed from a rotating earth which is assumed to be at rest.

The initial response to local forcing by wind stress is a rise of water level (set up) along the downwind shore and a fall (set down) along the upwind shore causing a positive surface slope upwind. The secondary response to the wind after the formation of set up and set down, known as a barotropic pressure gradient, is an upwind directed return flow occurring at near bottom layers. The bottom frictional force resists the upwind return flow. Therefore, a wind stress acting over the surface waters generates a relatively large internal vertical circulation as the surface waters are dragged in the direction of the wind with underlying water flowing in the opposite direction. Wind mixing significantly increases the vertical exchange of momentum, thereby reducing the density driven vertical circulation and stratification, and improves horizontal mixing.

The effectiveness of wind induced currents depends not only on the wind strength but also on the wind direction. The wind action at the free surface of a stably stratified water basin forms a turbulent upper layer, which deepens in time as denser water from the undisturbed layer is entrained into the upper layer. Between mixed and undisturbed layers, a thin interfacial layer can be distinguished. Buoyancy and horizontal velocity vary across the transition layer so that the turbulence is greatly suppressed by buoyancy differences. This entrainment phenomenon can significantly influence the vertical transport.

The movement of water is also influenced by daily and seasonal changes in climatic conditions; directly by the action of wind stress exerted on the water surface and indirectly by generating gravitational circulation induced by variations in the water density resulting from temperature and salinity differences. The characteristics of vertical distribution of temperature in the sea are: a mixed layer or homogeneous warm surface layer which is produced by absorption of solar radiation; the thermocline region in which the temperature decreases rapidly with depth from the mixed layer to the deep water below and the deep region in which the temperature falls very slowly with depth. Generally, coastal water bodies are not deep enough for the development of this structure. The term thermocline also applies to another region of abrupt change of temperature above the permanent thermocline and within the mixed layer. This shallower thermocline is referred to as seasonal thermocline and reflects the typical coupling between the air and sea at a particular season. There is also in certain regions, a diurnal thermocline, commonly known as afternoon effect, which reflects the daily thermal processes taking place at the air-sea boundary layer.

The density of sea water depends on both the temperature and the salinity. Therefore, all processes that alter the temperature or the salinity, influence the density. At the sea surface, the density is increased by cooling and evaporation. It is decreased by heating, condensation of water vapor, precipitation and freshwater runoff from land. As the solar radiation heats the surface layers of the water, the density in these layers decreases producing vertically stably-stratified conditions which inhibit vertical mixing. As the water surface cools at night or as the salinity increases caused by evaporation, unstable conditions can be created. The surface waters become denser and then tend to sink. This generates a vertical circulation, known as thermohaline convection. Horizontal density gradients caused by different rates of mixing or of different rates of heating because of variations in, for example, water depth, can generate large scale gravitational circulations.

Under stratified flow conditions, vertical excursions of a fluid element are damped by buoyancy forces, i.e. mixing lengths are reduced. Part of the turbulent kinetic energy carried by the fluid is converted to potential energy due to the mixing process. Thus, vertical turbulent fluxes under stratified conditions are much smaller than under neutral conditions. HYDROTAM 3D, is a three dimensional hydrodynamic and transport model that can simulate the coastal currents induced by wind and waves, density stratification due to changes in sea water temperature and salinity.

The governing equations in the three dimensional Cartesian coordinate system shown in Figure 1, are:

The continuity equation;

$$\frac{\partial u}{\partial x}+\frac{\partial v}{\partial y}+\frac{\partial w}{\partial z}=0 \qquad [4.1]$$

The momentum equations for the orthogonal horizontal directions x and y;

$$\frac{\partial u}{\partial t}+u\frac{\partial u}{\partial x}+v\frac{\partial u}{\partial y}+w\frac{\partial u}{\partial z}=fv-\frac{1}{\rho_0}\frac{\partial p}{\partial x}+2\frac{\partial}{\partial x}\left(v_x\frac{\partial u}{\partial x}\right)+\frac{\partial}{\partial y}\left(v_y\left(\frac{\partial u}{\partial y}+\frac{\partial v}{\partial x}\right)\right)+\frac{\partial}{\partial z}\left(v_z\left(\frac{\partial u}{\partial z}+\frac{\partial w}{\partial x}\right)\right) \qquad [4.2]$$

$$\frac{\partial v}{\partial t}+u\frac{\partial v}{\partial x}+v\frac{\partial v}{\partial y}+w\frac{\partial v}{\partial z}=-fu-\frac{1}{\rho_0}\frac{\partial p}{\partial y}+\frac{\partial}{\partial x}\left(v_x\left(\frac{\partial v}{\partial x}+\frac{\partial u}{\partial y}\right)\right)+2\frac{\partial}{\partial y}\left(v_y\frac{\partial v}{\partial y}\right)+\frac{\partial}{\partial z}\left(v_z\left(\frac{\partial v}{\partial z}+\frac{\partial w}{\partial y}\right)\right) \qquad [4.3]$$

and in the vertical direction z;

$$\frac{\partial w}{\partial t}+u\frac{\partial w}{\partial x}+v\frac{\partial w}{\partial y}+w\frac{\partial w}{\partial z}=-\frac{1}{\rho_0}\frac{\partial p}{\partial z}+gz+\frac{\partial}{\partial x}\left(v_x\left(\frac{\partial w}{\partial x}+\frac{\partial u}{\partial z}\right)\right)+\frac{\partial}{\partial y}\left(v_y\left(\frac{\partial w}{\partial y}+\frac{\partial v}{\partial z}\right)\right)+2\frac{\partial}{\partial z}\left(v_z\frac{\partial w}{\partial z}\right) \qquad [4.4]$$

where, x, y:horizontal coordinates, z:vertical coordinate, t:time, u,v,w:velocity components in x, y, z directions at any grid locations in space, vx, vy, vz:eddy viscosity coefficients in x, y and z directions respectively, f:corriolis coefficient, ρ(x,y,z,t): the in situ water density, ρo: the reference density, g:gravitational acceleration, p=pressure.

The density of sea water is a function of its salt content or salinity, its temperature, and to a lesser degree, its pressure. It is evident that, its distribution depends on the distribution of temperature and salinity. The average density of sea water is close to 1.0276 g/cm^3. The significant part of this number with respect to the density of other water samples is generally in and beyond the third decimal. Therefore, a convention has been adopted that instead of the density ρ, a quantity σt be used. The relation between two is;

$$\sigma_t=(\rho-1)\times 10^3 \qquad [4.5]$$

where ρ: density in gr/cm^3

The density increases noticeably with depth due to the increased hydrostatic pressure. This compression does not affect buoyancy or stability because all water masses moved up and down are similarly compressed. Therefore, the convention has been adopted to reduce all densities to σ_t (at 1 atm pressure), and to neglect compressibility in the equations of motion. Following formulae are used to calculate σ_t as a function of salinity and temperature:

$$S=1{,}80655\ Cl \qquad [4.6]$$

$$\sigma_t=\left(\sigma_o+0{,}1324\right)\left(1-A_t+B_t\left(\sigma_o-0{,}1324\right)\right)+\sum_t \qquad [4.7]$$

$$\sigma_o=-6{,}9\times 10^{-2}+1{,}4708\ Cl-1{,}57\times 10^{-3}\ Cl^2+3{,}98\times 10^{-5}\ Cl^3 \qquad [4.8]$$

$$A_t = 4,7867 \times 10^{-3}\ T - 9,8185 \times 10^{-5}\ T^2 + 1,0843 \times 10^{-6}\ T^3 \quad [4.9]$$

$$B_t = 1,803 \times 10^{-5}\ T - 8,146 \times 10^{-7}\ T^2 + 1,667 \times 10^{-8}\ T^3 \quad [4.10]$$

$$\Sigma_t = -(T - 3,98)^2\ (T + 283)\left(503,57\left(T + 67,26\right)\right)^{-1} \quad [4.11]$$

where, S:Salinity (%.) , Cl= Clorinity (gr/kg) , T: Temperature (^oC).

Model includes the thermohaline forcing. The temperature and salinity variations are calculated by solving the three dimensional convection-diffusion equations. Three dimensional convective diffusion equations which are used to determine the temperature, salinity is:

$$\frac{\partial Q}{\partial t} + u\frac{\partial Q}{\partial x} + v\frac{\partial Q}{\partial y} + w\frac{\partial Q}{\partial z} = \frac{\partial}{\partial x}\left(D_x\frac{\partial Q}{\partial x}\right) + \frac{\partial}{\partial x}\left(D_y\frac{\partial Q}{\partial y}\right) + \frac{\partial}{\partial z}\left(D_z\frac{\partial Q}{\partial z}\right) \quad [4.12]$$

where, D_x, D_y and D_z : turbulent diffusion coefficient in x,y and z directions respectively, Q: temperature (T), salinity (S).
The conservation of pollutant constituent is:

$$\frac{\partial C}{\partial t} + u\frac{\partial C}{\partial x} + v\frac{\partial C}{\partial y} + w\frac{\partial C}{\partial z} = \frac{\partial}{\partial x}\left(D_x\frac{\partial C}{\partial x}\right) + \frac{\partial}{\partial x}\left(D_y\frac{\partial C}{\partial y}\right) + \frac{\partial}{\partial z}\left(D_z\frac{\partial C}{\partial z}\right) + k_p C + S_s \quad [4.13]$$

where, C: pollutant concentration, k_p: decay rate of the pollutant concentration, S_s: Source of pollutant.

The kinematic condition at the free surface is;

$$\frac{\partial \eta}{\partial t} + u_s\frac{\partial \eta}{\partial x} + v_s\frac{\partial \eta}{\partial y} - w_s = 0 \quad [4.14]$$

where u_s, v_s: horizontal water particle velocities at the sea surface, w_s: vertical water particle velocity at the sea surface, η: water surface elevation.

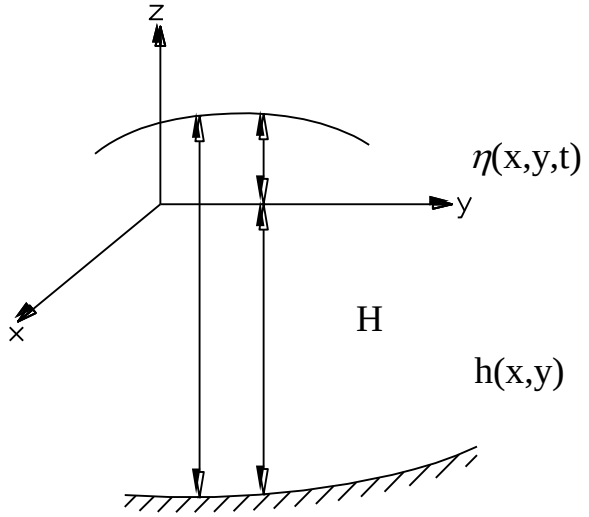

Figure 4. Definition sketch of water depth and water surface elevation in 3D Cartesian coordinate system

Integrating the continuity equation over the depth and using the kinematic condition at the free surface leads to the following free surface equation:

$$\frac{\partial \eta}{\partial t} + \frac{\partial}{\partial x}\left[\int_{-h}^{\eta} u\ dz\right] + \frac{\partial}{\partial y}\left[\int_{-h}^{\eta} v\ dz\right] = 0 \quad [4.15]$$

where h(x,y): water depth measured from the undisturbed water surface, H(x,y,t): total water depth, H(x,y,t)=h(x,y)+η(x,y,t).

To determine the horizontal pressure gradient terms that change with variable density, following equation is used;

$$p(x,y,z,t) = \int_z^\eta g\rho(x,y,z,t)\, dz \qquad [4.16]$$

Applying the Leibniz rule and dropping the independent variables gives,:

$$\frac{\partial p}{\partial x} = \frac{\partial}{\partial x}\int_z^\eta g\rho\, dz = \int_z^\eta g\,\frac{\partial \rho}{\partial x}\, dz + g\rho_s \frac{\partial \eta}{\partial x} \qquad [4.17]$$

ρ_s is the density at the surface. There is a corresponding expression for $\delta p/\delta y$.
Two equation k-ε turbulence model is used for turbulence modelling. The model equations for the kinetic energy and dissipation of kinetic energy are;.

$$\frac{\partial k}{\partial t} + u\frac{\partial k}{\partial x} + v\frac{\partial k}{\partial y} + w\frac{\partial k}{\partial z} = \frac{\partial}{\partial z}\left(\frac{v_z}{\sigma_k}\frac{\partial k}{\partial z}\right) + P + B - \varepsilon + \frac{\partial}{\partial x}\left(D_x\frac{\partial k}{\partial x}\right) + \frac{\partial}{\partial y}\left(D_y\frac{\partial k}{\partial y}\right) \qquad [4.18]$$

$$\frac{\partial \varepsilon}{\partial t} + u\frac{\partial \varepsilon}{\partial x} + v\frac{\partial \varepsilon}{\partial y} + w\frac{\partial \varepsilon}{\partial z} = \frac{\partial}{\partial z}\left(\frac{v_z}{\sigma_\varepsilon}\frac{\partial \varepsilon}{\partial z}\right) + C_{1\varepsilon}\frac{\varepsilon}{k}(P + C_{3\varepsilon}B) - C_{2\varepsilon}\frac{\varepsilon^2}{k} + \frac{\partial}{\partial x}\left(D_x\frac{\partial \varepsilon}{\partial x}\right) + \frac{\partial}{\partial y}\left(D_y\frac{\partial \varepsilon}{\partial y}\right) \qquad [4.19]$$

where, k: kinetic energy, ε: rate of dissipation of kinetic energy, v_x and v_y: horizontal eddy viscosities, v_z: vertical eddy viscosity, P: stress production of the kinetic energy, universal empirical constants; Cμ=0.09, σε=1.3, $C_{1\varepsilon}$=1.44, $C_{2\varepsilon}$=1.92. $C_{3\varepsilon}$=1 if G>0 and $C_{3\varepsilon}$= 0-0.2 if G<0 and B: buoyancy production of the kinetic energy, defined by;

$$B = \frac{g}{\rho_0}\frac{v_z}{Pr}\frac{\partial \rho}{\partial z} \qquad [4.20]$$

where *Pr*: Prandtl or Schmidt number. Experiments have shown that, the turbulent Prandtl or Schmidt number, varies only little across the flow and from flow to flow. Therefore, it is considered as a constant, *Pr* = 0.7.

Stress production of the kinetic energy, P is defined as the following;

$$P = v_h\left[2\left(\frac{\partial u}{\partial x}\right)^2 + 2\left(\frac{\partial v}{\partial y}\right)^2 + \left(\frac{\partial u}{\partial y} + \frac{\partial v}{\partial x}\right)^2\right] + v_z\left[\left(\frac{\partial u}{\partial z}\right)^2 + \left(\frac{\partial v}{\partial z}\right)^2\right] \qquad [4.21]$$

where v_h is the horizontal eddy viscosity.
Vertical eddy viscosity is calculated by;

$$v_z = C_\mu\frac{k^2}{\varepsilon} \qquad [4.22]$$

where; $C\mu$ is a universal empirical constant ($C\mu$ = 0.09)

The standard k-ε model assumes the local isotropy of the turbulence, where horizontal eddy viscosity is equal to the vertical eddy viscosity. If the horizontal motion has an intensity and length scale greater than the vertical motion, like in shallow water bodies, horizontal eddy viscosity can be simulated by the Smagorinsky algebraic subgrid scale turbulence model;

$$v_h = 0{,}01\Delta x\Delta y\left(\left(\frac{\partial u}{\partial x}\right)^2+\left(\frac{\partial v}{\partial y}\right)^2+\frac{1}{2}\left(\frac{\partial u}{\partial y}+\frac{\partial v}{\partial y}\right)^2\right)^{1/2} \quad [4.23]$$

According to the experimental results, the influence of stratification on turbulence in the horizontal direction is negligible. Hence the horizontal eddy diffusivities are estimated as equal to the horizontal eddy viscosities. Whereas, the vertical diffusivity, D_z, is expressed as:

$$D_z = \frac{v_z}{Pr} \quad [4.24]$$

There are mainly four type of boundaries which may appear in a physical problem; free surface, sea bed, open sea and coastal land boundaries.

Free Surface Boundary Condition

The shear stress at the free surface is given as:

$$\left[\tau_{wx},\tau_{wy}\right] = \rho_a C_d \left[u_w, v_w\right]\sqrt{u_w^2+v_w^2} \quad [4.25]$$

where, τ_{wx}, τ_{wy} : wind stress components in the x and y directions, respectively; u_w and v_w:wind velocity components (m/s), in the x and y directions, respectively; ρ_a :air density, C_d: drag coefficient of air.

In the literature, many formulations exist for the wind drag coefficient, ranging from a constant value for all wind speeds to complicated formulas taking into account the wind speed and direction, the roughness of the sea surface (wave height) and whether the sea state is fully developed or not. The following drag coefficient of air is used in the computations;

$$C_d = \begin{cases} 1.2 * 10^{-3} & W < 11 \text{ m/s} \\ (0{,}49 + 0{,}065\ W) * 10^{-3} & 11 \text{ m/s} \leq W < 25 \text{ m/s} \end{cases} \quad [4.26]$$

where, W: Wind speed.

The surface shear stress causes a vertical velocity gradient at the surface;

$$\tau_{wx} = \rho\nu_z \frac{\partial u}{\partial z}; \quad \tau_{wy} = \rho\nu_z \frac{\partial v}{\partial z} \quad [4.27]$$

At the free surface, the pollutant and salt fluxes are zero, whereas, the heat flux is:

$$D_z \frac{\partial T}{\partial z} = \frac{K}{\rho C_p}\left(T_s - T_e\right) \quad [4.28]$$

where, K: the surface heat transfer coefficient, ρ: fluid mass density, C_p: specific heat of water, T_s: surface temperature, T_e: equilibrium temperature.

The boundary conditions for the kinetic energy and its rate of dissipation also depend on surface shear. When wind stress is applied:

$$k_s = \frac{u_{*s}^2}{\sqrt{c_\mu}}; \qquad \varepsilon_s = \frac{\left|u_{*s}\right|^3}{\kappa\Delta z_s} \quad [4.29]$$

Otherwise,

$$\frac{\partial k_s}{\partial z} = 0; \qquad \varepsilon_s = \frac{\left(k_s \sqrt{C_\mu}\right)^{3/2}}{0{,}07\kappa H} \qquad [4.30]$$

where, u_{*s}: surface shear velocity, Δz_s: distance to the surface at the first grid point below the surface, c_μ:0,09, κ: 0,42 Karman constant, *H*: Total water depth.

Sea Bed Boundary Condition

At the sea bed, the shear stress is assumed to be a quadratic function of the bed velocity;

$$\tau_{bx} = \left[\nu_z \frac{\partial u}{\partial z} \right]_b = \rho_0 C_f u_b \sqrt{u_b^2 + v_b^2}; \qquad \tau_{by} = \left[\nu_z \frac{\partial v}{\partial z} \right]_b = \rho_0 C_f v_b \sqrt{u_b^2 + v_b^2} \qquad [4.31]$$

where, τ_{bx}, τ_{by}:bottom stress components in the x and y directions respectively; u_b, v_b:bottom velocity components in the x and y directions respectively; ρ_o: mean water density, C_f: empirical coefficient for bottom friction.

If sufficient resolution near the bottom boundary is provided, C_f can be estimated so that velocities match the logarithmic law of the wall;

$$C_f = \left(\frac{1}{\kappa} \ln\left(\frac{\Delta z_b}{z_0} \right) \right)^{-2} \qquad [4.32]$$

where, Δz_b: distance from the bottom to the grid point nearest the bottom; and z_0:parameter dependent on the local bottom roughness and set to 1 cm.

In those cases where bottom boundary layer is not well resolved, C_f is specified as a constant, typical of 0.002-0.003. The wall region is valid for $30<z^+<100$. In the spatial discretization, the first vertical mesh point should lie within this region. z^+ is calculated by;

$$z^+ = \frac{\Delta z_b u_{*b}}{\nu} \qquad [4.33]$$

u_{*b} is the bed friction velocity. The kinematic boundary condition at the sea bed;

$$w_b = -u_b \frac{\partial h}{\partial x} - v_b \frac{\partial h}{\partial y} \qquad [4.34]$$

The bottom turbulent kinetic energy k_b and dissipation ε_b ,are determined from the following relations:

$$k_b = \frac{u_{*b}^2}{\sqrt{C_\mu}}; \qquad \varepsilon_b = \frac{u_{*b}^3}{\kappa \Delta z_b} \qquad [4.35]$$

At the bottom of the basin, the normal gradients of the temperature, the salinity and the pollutant are zero so that there are no advective and diffusive heat and salt fluxes across the boundary.

Open Sea Boundary Condition

At the open sea boundary, velocities normal to the boundary are computed in the middle of the grid and horizontal gradient terms are treated accordingly.For the flows induced by tidal forces, following equations are used at the open sea boundary:

$$\eta = a_T \sin\left(2\pi \frac{t}{T_w}\right) \qquad [4.36]$$

$$V_n = (gh)^{1/2} a_T H^{-1} \cos\left(\frac{2\pi}{L_w}\frac{\Delta n}{2} + \frac{2\pi}{T_w}t\right) \qquad [4.37]$$

where, T_w and L_w: tidal period and tidal wave length respectively, V_n: depth mean velocity normal to the boundary, Δn:grid distance normal to the boundary, a_T: tidal amplitude.

Coastal Land Boundary Condition

The volume of water in a typical coastal system like lagoons shows seasonal variations, causing some water areas in the system to dry out or vice versa. Therefore, the boundaries of the coastal area need to be defined to simulate the flooding and drying processes. Once the free surface and new water velocities have been computed throughout the computational domain, before proceeding to the next time step, the total water depth and vertical grid spacings have to be updated. Since a negative value for the total water depth H, is physically meaningless, the discrete total depths $H_{i,j}$ are defined as:

$$H_{i,j} = \max\left(0, h_{i,j} + \eta_{i,j}\right) \qquad [4.38]$$

where; h(x,y): water depth from still water level and $\eta(x, y, t)$: water surface elevation.

Using a length scale L_b to characterize the bed roughness, the depth at the centre of each grid cell side is compared with L_b. If any total water depth becomes less than L_b or zero, this simply means a dry point which may be flooded when the total water depth becomes positive at a later time, and the corresponding velocity u or v across the side of the cell is forced to vanish. Thus, no flow is permitted across the grid cell side until the side is again flooded. It is important to point out that the resulting finite difference equation for the water surface elevation correctly accounts for positive and zero values of the total depth for a computational grid. The treatment of flooding and drying is borne out naturally without special treatment and guarantees mass conservation while accounting for the flooding and drying. The boundary shorelines, which may vary with time, are defined by the condition of no mass flux. At inflow boundaries, k and ε can be described from fully developed channel flow data as;

$$k = 0,004u_d^2 \qquad \varepsilon = c_\mu^{3/4} \frac{k^{3/2}}{0,09b_k} \qquad [4.39]$$

where, u_d: inflow velocity and b_k: inflow inlet width.

Equations are solved by approximating the horizontal gradient terms using staggered finite difference scheme. Whereas, in the vertical plane finite element Galerkin Method is applied. Water depths are divided into the same number of layers following the bottom topography. At all nodal points, the ratio of each element to the total depth is the same. By following the finite element approach, the values of velocities u, v, w; eddy viscosities, v_x, v_y, v_z; temperature, T; salinity, S; pollutant concentration, C; turbulent diffusion coefficients, D_x, D_y, D_z; kinetic energy, k; dissipation of kinetic energy, ε; pressure, p; at any point over the flow depth are written in terms of the values of

variables at vertical nodal points by using linear shape functions.

$$\tilde{\tilde{G}} = N_1 G_1^k + N_2 G_2^k \qquad [4.40]$$

$$N_1 = \frac{z_2 - z}{l_k}; \qquad N_2 = \frac{z - z_1}{l_k}; \qquad l_k = z_2 - z_1 \qquad [4.41]$$

where, $\tilde{\tilde{G}}$ is shape function, k is element number, N_1 and N_2 interpolation functions, l_k is the length of the k'th element, z_1 and z_2 are starting and end points of the k'th element, z is a variable that changes in between z_1 and z_2.

The approximate expressions for variables are substituted into the related equations. Since equations are not the exact solutions, there will be residuals in each of the equations. Resulting residual errors (R), are minimized using the Galerkin procedure. To increase the vertical resolution, whenever necessary, grid clustering can be applied in the vertical plane. Grids can be concentrated near the bottom, surface, or intermediate layers. After the application of Galerkin Method, any derivative terms with respect to horizontal coordinates appearing in the equations are replaced by central finite differences, considering unequal horizontal mesh sizes. Then, there occurs local matrices and vectors describing the nonlinear equations for each of the element over the water depth. The local element matrices for all elements on a vertical line are grouped together to form the global matrix equation for the unknown nodal time derivatives of the variables at a grid point on the horizontal plane. The sea bed and sea surface boundary conditions are taken into account, while building up the global matrices over the water depth. The mesh size may be varied in the horizontal plane. The details of the derivations are given in Balas and Özhan (2000).

The system of nonlinear equations is solved by the Crank Nicholson Method which is second order accurate in time. To provide this accuracy, difference approximations are developed at the midpoint of the time increment. The temporal first derivative is approximated at t+1/2 and all other variables and derivatives are determined by averaging the difference approximations at the beginning (t) and at the end(t+1) of the time increment. Resultant set of implicit equations are solved by iterative method, which is controlled by underrelation. Underrelaxation is typically employed to make a nonconvergent system converge or to hasten convergence by dampening out the oscillations.

After the estimation of horizontal velocities, the vertical velocities w, are calculated from the continuity equation, at each time step. The approximate expressions for horizontal velocities u and v, are substituted into the continuity equation:

$$\frac{\partial u}{\partial x} + \frac{\partial v}{\partial y} + \frac{\partial w}{\partial z} = 0 \qquad [4.42]$$

Residual error is minimized by the Galerkin method. Since the horizontal velocities are known, the equation to calculate the vertical velocity:

$$w_2^k = w_1^k - \frac{1}{2}\left[\frac{\partial l_k}{\partial x}\left(u_1^k - u_2^k\right) + l_k\left(\frac{\partial u_1^k}{\partial x} + \frac{\partial u_2^k}{\partial x} \right) + \frac{\partial l_k}{\partial y}\left(v_1^k - v_2^k\right) + l_k\left(\frac{\partial v_1^k}{\partial y} + \frac{\partial v_2^k}{\partial y} \right) \right]$$

$$-l_k\left[\left(u_1^k - u_2^k\right)\left(\frac{z_2}{l_k^2}\frac{\partial z_1}{\partial x} - \frac{z_1}{l_k^2}\frac{\partial z_2}{\partial x} \right) + \left(v_1^k - v_2^k\right)\left(\frac{z_2}{l_k^2}\frac{\partial z_1}{\partial y} - \frac{z_1}{l_k^2}\frac{\partial z_2}{\partial y} \right) \right] \qquad [4.43]$$

where; k=1, 2, m layer number and l_k is the length of the layer. Therefore, at each point, vertical velocities are computed implicitly, starting from the bottom layer to the surface layer, satisfying the continuity equation.

4.1. Suspendent Sediment Model

The governing three dimensional advection–diffusion equation (conservation equation) for suspended sediment where the vertical advection includes the particle settling velocity can be written as:

$$\frac{\partial C}{\partial t} + \underbrace{\frac{\partial (u.C)}{\partial x} + \frac{\partial (v.C)}{\partial y} + \frac{\partial (w.C)}{\partial z}}_{Advection} - \underbrace{\frac{\partial (w_s.C)}{\partial z}}_{Settling} = \underbrace{\frac{\partial}{\partial x}\left(D_x.\frac{\partial C}{\partial x}\right) + \frac{\partial}{\partial y}\left(D_y.\frac{\partial C}{\partial y}\right) + \frac{\partial}{\partial z}\left(D_z.\frac{\partial C}{\partial z}\right)}_{Diffusion} \qquad [4.1.1]$$

where,

C : Suspended sediment concentration,
t : Time,
x ,y : Horizontal coordinates,
z : Vertical coordinate,
u, v, : Velocity components in x, y and z directions at any grid locations in space respectively
w_s : Settling Velocity
D_x, D_y ,D_z : Turbulent diffusion coefficient in x, y and z directions respectively.

Settling Velocity

Initially, the setting velocity of sediment (w_s) is assumed to be constant in time and space. Settling motion of particles is effected by gravitational forces, viscous drag on particles and interparticle interactions. Thus, it is related to the sand grain size, kinematic viscosity of water and ratio of densities of particle and water. Due to the ability of forming flocs, the settling velocity for mud is generally not constant in time and space but strongly depends on turbulent intensity and the mud concentration in the water column. It is recommended to include and analyse the effect of a time- and space-dependent settling velocity for mud in a following phase (van Ledden, 2001).

For a given type of particles, the settling velocity may be derived from Stoke's formula for non-cohesive particles with a diameter less than 100 μm as follows:

$$w_s = \frac{(s-1).g.D_s^{\,2}}{18.\upsilon} \qquad [4.1.2]$$

w_s : Settling Velocity,
s : Ratio of densities of particles and water $\left(s = \frac{\rho_{sed}}{\rho_{water}}\right)$,
D_s : Representetive diameter of particles,
υ : Kinematic molecular viscosity of water,
g : Gravitational acceleration.

The particles that have representative diameter in the range of 64 μm and 250 μm is considered as very fine sand. If the particle diameter is less than 64 μm then, it is considered as cohesive mud (silt and clay). Cohesive sediments, subject to surface electrochemical forces and inter-particle collision because of their small size, will

flocculate, i.e. particles cluster in aggregates. As a result of floc aggregation, cohesive sediments settle by flocs rather than by individual particles (Teisson, 1991). It was found that the settling velocity of the flocs depended strongly on the suspended cohesive sediment concentration (Wu et al., 1999). At moderate concentrations, the settling velocity increases with concentration but, for higher concentration settling is hindered, because water has to be expelled through the interstitial spaces of the continuous network of aggregates.

4.2. Boundary Conditions

There are four types of boundaries; free surface, sea bed, open sea and coastal land boundaries. All boundary conditions are chosen to be time independent for reasons of simplicity.

4.2.1 Free Surface

The water velocity gradient below the sea surface is caused by wind induced shear stress at the sea surface:

$$\frac{\partial u}{\partial z}.\upsilon_z = \frac{\tau_{wind,x}}{\rho} \quad , \quad \frac{\partial v}{\partial z}.\upsilon_z = \frac{\tau_{wind,y}}{\rho} \qquad [4.1.3]$$

where, $\tau_{wind,x}$ and $\tau_{wind,y}$ are wind shear components in x and y directions; ρ is water density.

The wind induced shear stress at the sea surface is expressed as:

$$\left[\tau_{wx}, \tau_{wy}\right] = \rho_a.C_d.\left[u_w, v_w\right]\sqrt{u_w^{\,2} + v_w^{\,2}} \qquad [4.1.4]$$

where,

u_w,v_w : Wind velocity components (m/s) in x and y directions,
ρ_a : Air density,
C_d : Drag coefficient of air.

The formulation for drag coefficient:

$$C_d = \begin{cases} 1.2\times10^{-3} & W < 11m/s \\ \left(0.49 + 0.065\times W\right)\times10^{-3} & 11m/s \le W \le 25m/s \end{cases} \qquad [4.1.5]$$

where, W is the wind velocity (m/s).

The sea surface boundary condition for kinetic energy and its rate of dissipation when there exists wind shear is as follows:

$$k_s = \frac{u_{*s}^{\,2}}{\sqrt{C_\mu}} \quad ; \quad \varepsilon_s = \frac{\left\lfloor u_{*s} \right\rfloor^3}{\kappa.\Delta z_s} \qquad [4.1.6]$$

where,

u_{*s} : Surface shear velocity,
κ : von Karman constant (κ = 0.42),
Δz_s : Distance from the surface to the first grid point below.

Shear velocity is defined as:

$$u_{*sx} = \sqrt{\frac{\tau_{wx}}{\rho}} \qquad [4.1.7]$$

At the free surface the net vertical sediment flux was assumed to be zero, i.e. there is no exchange of particles through surface:

$$D_z \frac{\partial C}{\partial z} = \left[(w - w_s).C\right]_{surface} \qquad [4.1.8]$$

At the sea bed, the bottom shear stress is determined by matching velocities with the logarithmic law of wall:

$$\tau_{bx} = \left(\upsilon_z . \frac{\partial u}{\partial z}\right)_b = \rho_0 . C_f . u_b . \sqrt{u_b^{\,2} + v_b^{\,2}}$$

$$\tau_{by} = \left(\upsilon_z . \frac{\partial v}{\partial z}\right)_b = \rho_0 . C_f . v_b . \sqrt{u_b^{\,2} + v_b^{\,2}} \qquad [4.1.9]$$

where,

τ_{bx}, τ_{by} : The bottom shear stress components,

u_b, v_b : Horizontal velocity components at the grid point nearest to the sea bottom,

C_f : Empirical coefficient for bottom friction.

The sea bed boundary condition for kinetic energy and its rate of dissipation when there exists wind shear is as follows:

$$k_b = \frac{u_{*b}^{\,2}}{\sqrt{C_\mu}} \quad ; \quad \varepsilon_b = \frac{\left\lfloor u_{*b} \right\rfloor^3}{\kappa . \Delta z_b} \qquad [4.1.10]$$

It is assumed that, when bottom friction is smaller than a critical value for deposition, there is addition of matter to the bottom, and, when the bottom shear is higher than a minimum value, erosion occurs. Between those values, erosion and deposition balance each other.

At the bottom the boundary condition is that the fluxes of particles between the sea floor and water column is as flows:

$$-w_s . C_{bed} - D_z \frac{\partial C}{\partial z} = (E - D) \qquad [4.1.11]$$

Where D, E : Sediment transport rates through deposition and re-suspension, respectively

4.2.2. The Deposition Model

Deposition is calculated as the product of the settling flux and the probability of a particle to remain on the bed:

For $\tau \le \tau_d$ $\quad \dfrac{\partial M_D}{\partial t} = D = w_s(b).C(b).\left(1 - \dfrac{\tau_b}{\tau_d}\right)$

For $\tau > \tau_d$ $\quad \dfrac{\partial M_D}{\partial t} = D = 0$ $\qquad [4.1.12]$

where,

τ_d : Critical shear stress for deposition

$\left(1 - \dfrac{\tau_b}{\tau_d}\right)$: The probability of a settling particle becomes attached to the bed

The formulation is based on the assumption that a particle reaching the bottom has a probability of remaining there that varies between 0 and 1 as the bottom shear stress varies between its upper limit for deposition and zero, respectively. The critical shear stress for deposition depends mainly on size of particles/flocs. Bigger particles have higher probability of remaining on the bed than smaller particles. Nevertheless, previous works suggest that a constant value is a reasonable approximation (Caucino and Neves, 1999).

4.2.3. The Re-suspension Model

Erosion or re-suspension of bottom sediments is one of the most important factors controlling the fine sediment transport in natural water bodies. Far from lateral sources and sinks of materials, and in the absence of biological production, erosion is the major source for suspended particles in the water column. Re-suspension is a common physical process that occurs everywhere in the marine environment, both in shallow coastal areas and in the deep sea. Re-suspension occurs when shear stress (friction of the water against the bottom), is high enough to lift the sediment particles. Thus, re-suspension also leads to a transport of particles along the sea floor with currents. There is general agreement that bottom shear stress exerted by currents and waves are dominant forces causing re-suspension. Also, the site specific sediment characteristics like particle size distribution, particle density, cohesiveness, water content etc. control resistance to re-suspension. In the generally accepted re-suspension rate formulation of Partheniades, the site specific sediment characteristics are represented with erosion rate constant:

For $\tau \geq \tau_e$ $\quad \dfrac{\partial M_E}{\partial t} = E = ke.\left(\dfrac{\tau_b}{\tau_e} - 1\right)$

4.1For $\tau < \tau_e$ $\quad \dfrac{\partial M_E}{\partial t} = E = 0$ [4.1.13]

Critical shear stress for erosion is a function of the degree of compaction of bottom sediments measured by the dry density of the bottom sediments: ratio between the mass of sediment after extraction of the interstitial water at 105 C and its initial volume (Nicholson and O'Connor, 1986). In some applications threshold current velocities are used instead of critical shear stresses. One of the main difficulties in sediment transport modeling is the method of obtaining the re-suspension and deposition thresholds and the erodability constant. Thus, in previous applications they are selected by trial and error in such a way that they produce the best fit of model results to observations, although parameters must be physically realistic.

In the case of outgoing flux at the lateral boundaries and at bank boundaries, a Neumann condition is imposed:

$$\frac{\partial C}{\partial x} = 0 \quad ; \quad \frac{\partial C}{\partial y} = 0 \qquad [4.1.14]$$

For inflow conditions at the open boundaries, the concentrations have to be specified. At open sea boundaries, generally a value of concentration is imposed. At coastal land boundaries, in the case of inflow flux condition, an equilibrium sand concentration profile is used.

5. **Wind and Wave Climate Sub Models**

Estimation of the wind climate that provides detailed information about the wind properties of the region, is crucial in almost all of the coastal and marine projects. In the database of HYDROTAM 3D, hourly measured wind data collections (wind speed and direction) of all the coastal Turkish Meteorological Stations are available between the years of 1970-2018. The locations of all the coastal Turkish Meteorological Stations are shown on the map of Turkey based on Geographic Information System. As well ECMWF operational and ERA archive (2000-2018) six hourly wind and wave predictions are also avaliable on a mesh covering Turkish coastline with a resolution of 0.1^{o}x0.1^{o} in the data base for analysis. The user can select the coastal study area on the map and can select the relevant nearest Meteorological Station or ECMWF operational and ERA archive wind data. Firstly, wind characteristics of the area are analyzed. Storm periods are investigated. The yearly, seasonal and monthly wind roses, which provide the directional distribution of wind speeds, are obtained. Maximum wind speeds and related directions are analyzed and dominant wind direction for the area is identified.

Yearly wind rose shows the number of occurrences of winds blowing with different speeds and from different directions during the period of measurements of Meteorological Stations. The main wind directions showing from which direction wind blows, are selected as the main geological directions. These directions start from the North (N), and moves in clockwise direction as, N (North), NNE (NorthNorthEast), NE (NorthEast), ENE (EastNorthEast), E (East), ESE (EastSouthEast), SE (SouthEast), SSE (SouthSouthEast), S (South), SSW (SouthSouthWest), SW (SouthWest), WSW (WestSouthWest), W (West), WNW (WestNorthWest), NW (NorthWest), NNW (NorthNorthWest). Wind speeds are listed in the colored scale next to the wind rose. The numbers of occurrences of each wind speed intervals are shown in the wind rose. In a similar manner, seasonal wind roses are presented by analyzing the hourly wind data of only winter, spring, summer or autumn seasons.

Winter season covers the hourly data of December, January and February; spring season covers the hourly data of March, April, and May; summer season covers the hourly data of June, July and August; autumn season covers the hourly data of September, October and December. The monthly mean and maximum wind speeds are depicted on a graph. The monthly mean of the wind speeds is calculated by averaging the hourly wind speeds in that month between the years of measurements in each of the Stations (1970-2018). As the monthly extreme wind speeds, the maximum, the minimum and the average wind speeds of the highest wind speeds observed in that month for each of the years in the measurement period (for each of the months, averaging the highest wind speed in that month in every years of the measurement period) are given.

As the wind statistics, “long term” and “extreme value” statistics are applied. Long term statistics use all of the hourly wind data measured in the measurement period of 1970-2018, that is continuous. Long term statistics is based on log-normal probability distributions. For each of the wind directions, the probability of exceedences of each wind speeds are presented. From a pre-specified direction, how many hours a pre-specified wind speed will be exceeded in a year are calculated.

In the extreme value wind statistics, the highest wind speeds in each year in the measurement period of the Meteorological stations (1970-2018) are used. The yearly

highest wind speeds are investigated statistically by Gumbel Probability distribution and presented graphically on the Gumbel papers. The best line is fitted to the wind speeds on the Gumbel paper and extrapolation for a higher value is also possible. On the upper horizontal axis, the return periods of all wind speeds are also given.

The knowledge of wind and wave characteristics is essential for almost any engineering activity in coastal waters. In many applications, it is necessary to use long-term wind and wave data. However, like in many areas, in Turkey, long-term wave measurements are not available and it is necessary to use wave prediction models for wave hindcasting. During the past decades, some empirical and numerical models have been developed for wave prediction. Numerical models, which solve the energy balance equation, require abundant bathymetric, meteorological and oceanographic data. In some regions, these data are not available and numerical modeling is both difficult and expensive. Besides, many numerical models have problems in producing accurate results in some coastal areas, such as the Aegean Sea and the Sea of Marmara coasts of Turkey, where the coastal land boundary may not be represented well due to the limitations in computational mesh size.

Therefore, in many coastal engineering projects, engineers tend to use simplified empirical wave prediction methods that base on interrelationships between dimensionless parameters. There are several empirical wave prediction methods that have been developed and verified with the measurements in the past decades SMB (Bretschneider,1970), JONSWAP (Hasselmann et al. 1976), SPM (US Army, 1984), CEM (US Army, 2006).

The wave parameters, significant wave height (Hs) and corresponding wave period (Ts), are estimated by CEM empirical method. For this purpose, wind speed measurements are converted to wind speeds at 10 m height and the fetch lengths are determined for the point of concern. Effective fetch lengths are calculated by the cosine average method. For a certain direction, the average of fetch distances in the $\pm 22.5^{o}$ interval with 7.5^{o} increments is computed and assigned as the effective fetch length of that direction;

$$X_{ef} = \frac{\sum X_i \cos^2 \theta_i}{\sum \cos \theta_i} \qquad [5.1]$$

where X is the fetch length and X_{ef} is the effective fetch length.

WAM numerical model is a third generation wave model, which computes spectra of random short-crested wind-generated waves, being one of the most popular and well tested wave models (WAMDI Group-WAve Model Development and Implementation, 1988). Predicted significant deep water heights and periods at every 0.1 degree horizontal grid spacing and 6 hour time intervals covering all of Turkish coastal waters between years 2000-2018 by WAM model (ECMWF ERA-interim wave data), exists in the database.

Thus, the long-term wave climate of the area are studied utilizing the wave heights, wave periods and wave directions, estimated from the hourly wind data and fetch lengths by CEM method or from the wave data predicted by WAM. Yearly and seasonal wave roses are prepared. The monthly mean significant wave heights are computed as

the average of all significant wave heights occurred in a given month during the investigation period. The monthly peak wave heights during the same period are collected and the lowest, highest and mean values of those peaks are determined. The relation between the significant wave heights and the wave periods is observed to estimate the range of wave periods associated with a given wave height.

The predicted significant wave heights are used in the long term and extreme value wave statistics. In the long term wave statistics all of the predicted continuous wave data corresponding to the period of wind measurements are used. There are various probability distributions used for the long-term wave climate studies. Among them, the log-normal probability distribution is used in the model that is widely used to represent the durations of exceedences for the significant wave heights from each direction. The graphs of significant wave heights, Hs and their exceeding probabilities, P(>Hs) for every propagation direction are prepared. Then wave rose of the region is prepared that shows the long-term distribution of wave height and direction. Log-normal probability distribution equation is as follows;

$$Q(H_{1/3})=e^{2,3(H1/3-B)/A} \quad [5.2]$$

In the equation; $Q(H_{1/3})$ is the exceedence or being equal probability of predicted wave height to $H_{1/3}$, $H_{1/3}$ is the significant wave height, A and B are distribution parameters.

Log-normal probability distribution can be written in the following form:

$$H_{1/3}=A*LogQ(H_{1/3})+B \quad [5.3]$$

The log-normal probability graphs of significant wave heights are prepared for every propagation direction. The exceedence probability of any specified wave height is listed in terms of hours per year.

Using the predicted wave data, yearly and seasonal wave roses are prepared. Wave roses show the occurrence number of significant wave heights from each of the wave propagation directions yearly, seasonally or monthly. Wave propagation directions are chosen to be the same as 16 main geographical directions. The sea state is accepted as calm, if the wave height is calculated to be less than 0.5 meters. If the sea state is calm, direction of the wave is assumed to be negligible, and occurrence probability is given in the circle located in the middle of the wave rose. It is possible to decide the dominant and secondary wave propagation directions for the project site from the wave roses.

Extreme value statistics is also applied to the predicted significant wave heights. The highest significant wave heights of each year is fitted to the Gumbel probability distribution and presented graphically on the Gumbel papers. The best line is fitted to the significant wave heights on the Gumbel paper, extrapolation for higher values are also possible. On the upper horizontal axis, the return periods of all wave heights are also given.

6. Wave Propagation Submodel

Model equations similar to that proposed by Ebersole (1985) are solved numerically to deal with the combined refraction diffraction problem. The mild slope equation has been decomposed into three equations related to wave phase function, wave amplitude and wave approach angle that computes the wave field resulting from the transformation of an incident, linear wave as they propagate over irregular bottom configurations.

Proposed model does not have the limitation that one coordinate should follow the dominant wave direction. Different wave approach angles can be investigated on the same computational grid. Finite difference approximations with variable mesh sizes are used to solve governing equations. Finer grid resolution can be generated in areas of complex bathymetry. The use of variable grid sizes considerably reduces the overall computational costs. Computationally, the numerical model is quite efficient for simulating wave propagation over large coastal areas subjected to varying wave conditions (Inan and Balas, 2002).

The complex velocity potential has been chosen as (Ebersole, 1985)

$$\phi = a e^{is} \qquad [6.1]$$

in which, a: wave amplitude, s: scalar phase function of the wave.

If Eqn (47) is inserted to the equation that describes the propagation of harmonic linear waves in two horizontal dimensions, the following equation can be derived;

$$\frac{1}{a}\left[\frac{\partial^2 a}{\partial x^2}+\frac{\partial^2 a}{\partial y^2}+\frac{1}{CC_g}\left(\nabla a\cdot\nabla\left(CC_g\right)\right)\right]+k^2-\left|\nabla s\right|^2=0 \qquad [6.2]$$

$$\nabla(a^2 CC_g \nabla s)=0 \qquad [6.3]$$

in which ∇: horizontal gradient operator; C: wave celerity; C_g: group velocity; k: wave number calculated by the dispersion relation.

From vector analysis, the normal unit vector n to a scalar function is related to the normal vector N, which is found by taking the gradient of the function (Dean and Dalrymple, 1991);

$$N = n\left|\nabla s\right| \qquad [6.4]$$

The vector N points in the direction of the greatest change of phase function s, which is the wave propagation direction. The wave number vector $\vec{k}$ is defined as;

$$\vec{k} = n\left|\nabla s\right| = \nabla s \qquad [6.5]$$

It is clear that the wave number vector is nothing more than the wave number oriented in the wave direction. To account the effect of diffraction, the wave phase function changes to consider any horizontal variation in the wave height. By the use of irrotationality of the gradient of the wave phase function following equations can be derived;

$$\nabla\times(\nabla s)=0 \qquad [6.6]$$

$$\nabla s = \left|\nabla s\right|\cos(\theta)\vec{i} + \left|\nabla s\right|\sin(\theta)\vec{j} \qquad [6.7]$$

in which $\vec{i}$, $\vec{j}$: unit vectors in the x and y directions, respectively; θ(x,y): angle of incidence defined as the angle made between the bottom contour normal and the wave direction. θ(x, y) can be found from the following expression;

$$\frac{\partial}{\partial x}(\left|\nabla s\right|\sin\theta)-\frac{\partial}{\partial y}(\left|\nabla s\right|\cos\theta)=0 \qquad [6.8]$$

The following energy equation is used to determine wave amplitude;

$$\frac{\partial}{\partial x}\left(a^2 CC_g |\nabla s| \cos\theta\right)+\frac{\partial}{\partial y}\left(a^2 CC_g |\nabla s| \sin\theta\right)=0 \qquad [6.9]$$

Eqn (6.6) together with Eqn (6.2) and Eqn (6.7) result in the set of three equations that will be solved in terms of three wave parameters, wave height H, local wave angle θ and $|\nabla s|$ (Ebersole, 1985).

$$|\nabla s|=k^2+\frac{1}{H}\left[\frac{\partial^2 H}{\partial x^2}+\frac{\partial^2 H}{\partial y^2}+\frac{1}{CC_g}\left(\frac{\partial H}{\partial x}\frac{\partial CC_g}{\partial x}+\frac{\partial H}{\partial y}\frac{\partial CC_g}{\partial y}\right)\right] \qquad [6.10]$$

$$\frac{\partial}{\partial x}\left(H^2 CC_g |\nabla s| \cos\theta\right)+\frac{\partial}{\partial y}\left(H^2 CC_g |\nabla s| \sin\theta\right)=0 \qquad [6.11]$$

Eqns (6.8), (6.10) and (6.11) describe the refraction and diffraction phenomena. The basic assumptions are that the waves are linear, harmonic, irrotational, reflection is neglected and bottom slopes are small.

Solution method is a finite difference method that uses a mesh system in Cartesian coordinates. The finite difference approximations can handle the variations in the horizontal mesh sizes. The horizontal mesh size Δx in the x-coordinate is orthogonal to the horizontal mesh size Δy in the y-coordinate. The horizontal mesh sizes Δx and Δy can be different from each other. Also, Δx can vary along the x coordinate and Δy can vary along the y coordinate (Inan and Balas, 2002, Balas and İnan, 2001a; Balas and İnan, 2001b).

Input model parameters are the deep water wave parameters, wave height (H_0), wave approach angle (θ_0) and the wave period (T). Partial derivatives in the x-direction are expressed by forward finite differences of order O(Δx), and the partial derivatives in the y-direction are expressed by central finite differences of order O(Δy^2) in equation (6.8) and in Equation (6.11), whereas partial derivatives in the x-direction are approximated with backward finite differences of order O(Δx), and partial derivatives in the y-direction are expressed by central finite differences of order O(Δy^2) in Equation (6.10). Wave breaking is controlled during the computations (Inan and Balas, 2002).

7. **Longshore Sediment Transport Submodel**

In coastal zones, current pattern changes due to natural (climate change) or artificial (coastal structures), these changes cause sediment transport so coastal erosion or deposition ocur. The main effect on longshore transport is currents depending on wave breaking. Sediment transport modeling includes these works:

- Determination of wave climate
- Modeling of wave transformations
- Determination of current pattern
- Determination of direction of sediment transport, the amount of transport of sediment
- Studying on the effects of sediment transport on the coastal structures

Developed sediment transport model cover the basic equations (Yegul, 2005)

Conservation of mass: Predictions of current velocities and sediment concentration are calculated considering turbulence effects.
Equation of motion: The effects of suspended sediment on transport are investigated.
Equation of sediment transport: The sediment movement in horizontal and vertical directions, distribution and settling of sediment are analyzed.

Before solving the equations, sediment diameter, density of sediment, critical shear stress, bottom shear stress, settling velocity should be determined. Sediment transport, sediment deposition and erosion in coastal zones effect on hydrodynamics of the coastal system. High amount of sediment deposition can change flow regime. The model is adaptable to morphological changes. Developed longshore sediment model is based on long term wave statistics. Occurence probability for each direction is considered in the model. Net and gross longshore sediment transport rate are calculated with the CERC method (US Army, 2006).

In this submodel, the changes along the shore in the effect of waves are simulated. Longshore sediment transport model can consider wave properties depending on time and location, breakwaters, seawall, groins etc.
Advantages

- All kind of coastal fill and construction can be modeled.
- Different types of structures like T groins, combined breakwaters can be taken into account.
- Sediment transport around piers and groins can be prevented or allowed.
- The model consider wave refraction, wave diffraction and reflection due to berakwaters, groins and piers.
- Wave transmission through breakwaters can be allowed.
- The effects of waves coming from different direction with various wave heigths and periods.
- Many combination of waves can be included.

Disadvantage

- Evaluation of a tombolo cannot be taken into account.

Longshore energy flux P_{ls} is calculated with the equation (7.1).

$$P_{ls} = E_{fb}\, C_{gb} \cos(\alpha_b)\sin(\alpha_b) \qquad [7.1]$$

Where P_{ls} : Longshore energy flux ; E_{fb} : Wave energy at breaking; α_b : Incidence wave angle at breaking; C_{gb} : Group velocity at breaking

Wave energy and group velocity in breaking condition are given in Equation (7.2) and (7.3), respectively.

$$E_{fb} = \frac{1}{8} g \rho H_B^2 \qquad [7.2]$$

Where, g: Gravitational acceleration; H_B : Breaking wave height; ρ Seawater density

$$C_{gb} = \sqrt{g d_b} \qquad [7.3]$$

d_b : Breaking depth

Volumetric transport rate , Q_l can be calculated using longshore energy flux.

$$Q_l = P_{ls}\ 8{,}16 \times 10^{-5} \qquad [7.4]$$

Amount of sediment transport can be calculated using volumetric transport rate and physical properties of the sediment as shown in Equation (7.5).

$$I_l = (\frac{\rho_s}{\rho} - 1)g(1-n)Q_l \quad [7.5]$$

ρ_s/ρ : Ratio between sediment density water density, g: Gravitational acceleretion, n: Porosity.

If equation (7.4) and sediment properties are substituted in equation (7.5), then equation (7.6) is obtained for calculating sediment transport rate in Nt/sec.

$$I_l = 39{,}62 \times 10^{-5} E_{fb} C_{gb} \sin(2\alpha_b) \quad [7.6]$$

8. Water Quality Component

The water quality component of HYDROTAM 3D is a zero dimensional ecological model based on the conservation equations and formulations proposed by the United States Environmental Protection Agency in 1985 (EPA, 1985). Biochemical cycles simulated in the model are the cycles of nitrogen, phosphorus, and oxygen. Organisms simulated in the model are the low tropic levels in aquatic environments i.e. phytoplankton, zooplankton and pelagic bacteria (Cebe and Balas, 2016; Cebe and Balas, 2018).

The rate of change of the water quality parameters are developed by assuming a homogenous distribution of all properties throughout the computation cell and can be generalized as follows:

$$\frac{\partial C}{\partial t} + \nabla \cdot (aC) = \sigma \quad [8.1]$$

where, σ is the sum of the internal sink and sources of the water quality parameter in mg/l/day.

For n number of neighboring computational cells, the formula can be extended as follows:

$$\frac{\partial C}{\partial t} = a_1 . \frac{\partial C}{\partial x_1} + a_2 \frac{\partial C}{\partial x_2} ... + a_n \frac{\partial C}{\partial x_n} + S_i - [K]C \quad [8.2]$$

where, C is the concentration of the water quality parameter in mg/l, a_i is the rate of exchange with neighboring computational cell in m/day, S_i is the source of pollution for cell "i" in mg/l/day, K is the internal rate of change of the water quality parameter.

Nitrogen Cycle

Nitrogen cycle in marine environment is one of the important phenomena since it is closely related with primary production and eutrophication problem. In water quality model nitrogen cycle is demonstrated with basic steps of the cycle which can be summarized in the schematic figure 4

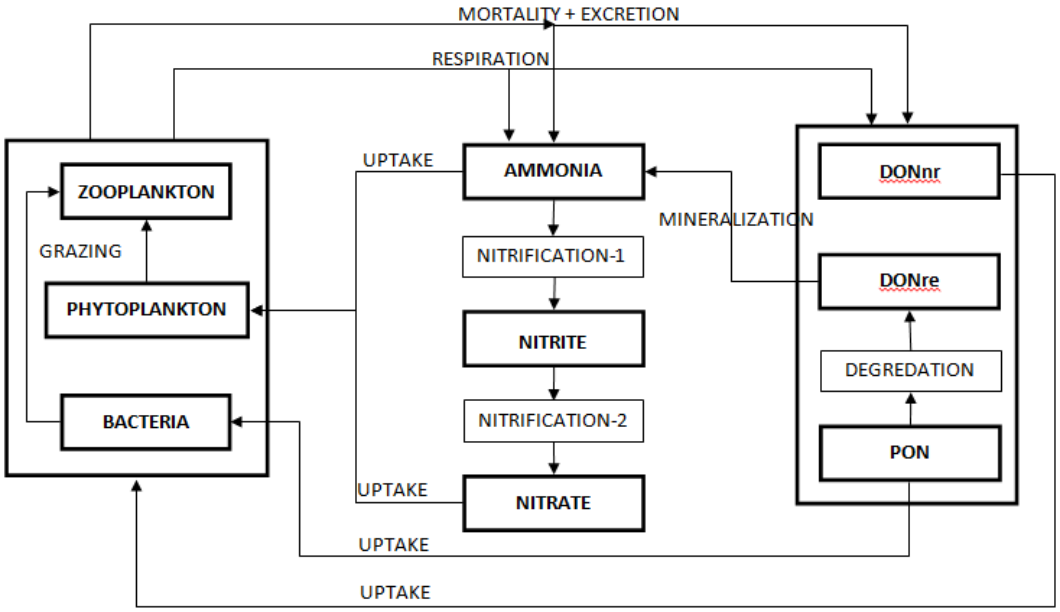

Fig 4: Nitrogen Cycle in Marine Environment

The forms of nitrogen in marine environment demonstrated in the water quality model are ammonia (NH_4^-), nitrite (NO_2^-), nitrate (NO_3^-), particulate organic nitrogen (PON), non-refractory dissolved organic nitrogen (DONnr) and refractory dissolved organic nitrogen (DONre) .

Ammonia

Main sources of ammonia in marine environment are represented in the model as follows:

a. Inorganic matter from the excretion and respiration of phytoplankton,
b. Excretion of pelagic bacteria,
c. Inorganic matter from the excretion of zooplankton,
d. Inorganic matter from the respiration of zooplankton.
e. Mineralization of the refractory dissolved organic nitrogen.

Main sinks of ammonia in marine environment are represented in the model as follows:

a. Uptake by phytoplankton,
b. Uptake by pelagic bacteria,
c. Nitrification of ammonia.

The rate of change in ammonia concentration can be formulized as follows:

$$\frac{\partial C^{NH4}}{\partial t} = \begin{cases} \left[f_{in}^{f} \cdot \left(e^{f} + r^{f} \right) - \beta_{NH4}^{f} \cdot \mu^{f} \right] \cdot \alpha_{N:C}^{f} \cdot C^{f} \\ + \left[e^{b} - \mu_{NH4}^{b} \right] \cdot \alpha_{N:C}^{b} \cdot C^{b} \\ + \left[f_{in}^{z} \cdot e^{z} + r^{z} \right] \cdot \alpha_{N:C}^{z} \cdot C^{z} \\ + K_{\min}^{DONre} \cdot C^{DONre} \\ - K_{nit}^{NH4} \cdot C^{NH4} \end{cases} \quad [8.3]$$

where, f^{f}_{in} is the fraction of inorganic matter excreted from phytoplankton, f^{z}_{in} is the

fraction of inorganic matter excreted from zooplankton, β^f_{NH4} is the ammonia preference factor in phytoplankton uptake, $\alpha^f_{N:C}$ is the nitrogen to carbon ratio for phytoplankton in mgN/mgC, $\alpha^b_{N:C}$ is the nitrogen to carbon ratio for bacteria in mgN/mgC, $\alpha^z_{N:C}$ is the nitrogen to carbon ratio for zooplankton in mgN/mgC, K^{DONre}_{min} is the rate of mineralization in 1/day and K^{NH4}_{nit} is the nitrification rate in 1/day.

Ammonia preference factor in phytoplankton uptake is formulized as a function of the concentrations of the nutrients as follows (EPA, 1985):

$$\beta^f_{NH4} = \left(\frac{C^{NH4}}{K^f_N + C^{NH4}}\right)\cdot\left(\frac{C^{NO3}}{K^f_N + C^{NO3}}\right) + \left(\frac{C^{NH4}}{C^{NH4} + C^{NO3}}\right)\cdot\left(\frac{K^f_N}{K^f_N + C^{NO3}}\right) \quad [8.4]$$

where, K^f_N is the nitrogen half-saturation constant for phytoplankton uptake in mgN/l.

Mineralization and nitrification are formulized as half-saturation functions as shown below (EPA, 1985):

$$K^{DONre}_{\min} = K^{DONre}_{\min}(T_{ref})\cdot\left(Q^{DONre}_{\min}\right)^{(T-T_{ref})}\cdot\frac{C^f}{K^f_r + C^f} \quad [8.5]$$

$$K^{NH4}_{nit} = K^{NH4}_{nit}(T_{ref})\cdot\left(Q^{NH4}_{nit}\right)^{(T-T_{ref})}\cdot\frac{C^O}{K^{sat}_{nit} + C^f} \quad [8.6]$$

Where, $K^{DONre}_{min}(T_{ref})$ is the mineralization rate for refractory dissolved organic nitrogen at reference temperature (T_{ref}) in 1/day, $K^{NH4}_{nit}(T_{ref})$ is the nitrification rate for ammonia at reference temperature (T_{ref}) in 1/day, Q^{DONre}_{min} is the temperature constant for mineralization of refractory dissolved organic nitrogen, K^f_r is the half-saturation rate for mineralization in mgC/l, Q^{NH4}_{nit} is the temperature constant for nitrification of ammonia, C^O is the concentration of oxygen in mgO_2/l and K^{sat}_{nit} is the half-saturation constant for nitrification in mgO_2/l.

Nitrite

The rate of change in nitrite concentration is formulated as follows:

$$\frac{\partial C^{NO2}}{\partial t} = K^{NH4}_{nit}\cdot C^{NH4} - K^{NO2}_{nit}\cdot C^{NO2} \quad [8.7]$$

where K^{NO2}_{nit} is the nitrification rate of nitrite in 1/day.

Similar to the nitrification rate for ammonia, nitrification rate for nitrite can be expressed as follows (EPA,1985):

$$K^{NO2}_{nit} = K^{NO2}_{nit}(T_{ref})\cdot\left(Q^{NO2}_{nit}\right)^{(T-T_{ref})}\cdot\frac{C^O}{K^{sat}_{nit} + C^O} \quad [8.8]$$

where, $K^{NO2}_{nit}(T_{ref})$ is the nitrification rate for nitrite at reference temperature (T_{ref}) in 1/day, Q^{NO2}_{nit} is the temperature coefficient for nitrification of nitrite.

Nitrate

The rate of change in nitrite concentration is formulated as follows:

$$\frac{\partial C^{NO3}}{\partial t} = -(1-\beta^f_{NH4})\cdot\mu^f\cdot\alpha^f_{N:C}\cdot C^f + K^{NO2}_{nit}\cdot C^{NO2} - K_{dnit}\cdot C^{NO3} \quad [8.9]$$

where, K_{dnit} is the rate of denitrification in 1/day. Similar to the nitrification rates, the denitrification rate is calculated as an half-saturation function as follows :

$$K_{dnit} = K_{dnit}(T_{ref}) \cdot \left(Q_{dnit}\right)^{\left(T-T_{ref}\right)} \cdot \frac{K_{dnit}^{sat}}{K_{dnit}^{sat} + C^{O}} \quad [8.10]$$

Where, $K_{dnit}(T_{ref})$ is the denitrification rate at reference temperature in 1/day, Q_{dnit} is the temperature coefficient for denitrification and K^{sat}_{dnit} is the half saturation constant for denitrification in mgO_2/l.

Particulate Organic Nitrogen (PON)

The sources for particulate organic nitrogen in marine environment are:

a. particulate organic fraction of matter produced by excretion,
b. respiration and mortality of the phytoplankton,
c. particulate matter produced by mortality of the pelagic bacteria,
d. particulate fraction of the matter that cannot be assimilated through grazing of phytoplankton and bacteria by zooplankton and the stoichiometric losses,
e. particulate organic fraction of matter produced by excretion, mortality and grazing of the zooplankton.

The sinks for particulate organic nitrogen can be summarized as follows:

a. Uptake by pelagic bacteria,
b. Degradation to dissolved organic nitrogen.

The rate of change in particulate organic nitrogen concentration can be formulized as follows:

$$\frac{\partial C^{PON}}{\partial t} = \begin{cases} \left[\left(1-f_{in}^{f}\right)\cdot\left(1-f_{orgD}^{f}\right)\cdot\left(e^{f}+r^{f}\right)+m^{f}\right]\cdot\alpha_{N:C}^{f}\cdot C^{f} \\ -\left(\mu_{PON}^{b}-m^{b}\right)\cdot\alpha_{N:C}^{b}\cdot C^{b} \\ +\left[\left(1-f_{in}^{z}\right)\cdot\left(1-f_{orgD}^{z}\right)\cdot e^{z}+m^{z}+p^{z}\right]\cdot\alpha_{N:C}^{z}\cdot C^{z}+\left(\delta_{N}^{z}+\varphi_{N}^{z}\right)\cdot C^{z} \\ -(1-f_{orgp})\cdot K_{dec}^{PON}\cdot C^{PON} \end{cases} \quad [8.11]$$

where, δ^{z}_{N} is the rate of production of the particulate fraction of the matter that cannot be assimilated by grazing of phytoplankton and bacteria by zooplankton in 1/day, $\varphi^{z}_{N}$is the rate of the stoichiometric losses in 1/day, f_{orgp} is the fraction of the particulate organic nitrogen available for mineralization and K^{PON}_{dec} is the rate of degradation of the particulate organic nitrogen in 1/day.

The rate of production of the particulate fraction of the matter that cannot be assimilated by grazing of phytoplankton and bacteria by zooplankton is formulated as follows:

$$\delta_{N}^{z} = \left(1-E^{f}\right)\cdot\alpha_{N:C}^{f}\cdot C_{z}^{f} + \left(1-E^{b}\right)\cdot\alpha_{N:C}^{b}\cdot C_{z}^{b} \quad [8.12]$$

where, C^{f}_{z} is the assimilation rate of the phytoplankton by zooplankton in 1/day, C^{b}_{z} is the assimilation rate of the bacteria by zooplankton in1/day, E^{f} is the assimilation efficiency of the phytoplankton by zooplankton and E^{b} is the assimilation efficiency of the bacteria by zooplankton.

The rate of the stoichiometric losses are formulated as follow:

$$\varphi_{N}^{z} = \left(\alpha_{N:C}^{f}-\alpha_{N:C}^{z}\right)E^{f}\cdot C_{z}^{f} + \left(\alpha_{N:C}^{b}-\alpha_{N:C}^{z}\right)E^{b}\cdot C_{z}^{b} \quad [8.13]$$

Where, $\alpha^{f}_{N:C}$ is the ratio of nitrogen to carbon for phytoplankton in mgN/mgC, $\alpha^{b}_{N:C}$ is the ratio of nitrogen to carbon for bacteria in mgN/mgC and $\alpha^{z}_{N:C}$ is the ratio of nitrogen to carbon for zooplankton in mgN/mgC.

The rate of degradation of particulate organic nitrogen is defined as a temperature limiting function and formulated as follows:

$$K_{dec}^{PON} = K_{dec}^{PON}(T_{ref}) \cdot Q_{dec}^{(T-T_{ref})} \quad [8.14]$$

where, $K^{PON}_{dec}(T_{ref})$ is the degradation rate of PON at reference temperature (T_{ref}) in 1/day, Q_{dec} is the temperature constant for degradation.

Non-refractory Dissolved Organic Nitrogen (DONnr)

Sources of the non-refractory dissolved organic nitrogen (DONnr) are the dissolved fraction of the organic matter produced by the excretion and the respiration of the phytoplankton. The sink of the non-refractory dissolved organic nitrogen is the bacterial uptake. The rate of the change in the non-refractory dissolved organic nitrogen is formulated as follows:

$$\frac{\partial C^{DONnr}}{\partial t} = \begin{cases} (1-f_{in}^{f}) \cdot f_{orgD}^{f} \cdot (e^{f} + r^{f}) \cdot \alpha_{N:C}^{f} \cdot C^{f} \\ -\mu_{DONnr}^{b} \cdot C^{b} \\ +(1-f_{in}^{z}) \cdot f_{orgD}^{z} \cdot e^{z} \cdot \alpha_{N:C}^{z} \cdot C^{z} \end{cases} \quad [8.4]$$

where, μ^{b}_{DONnr} is the uptake rat of the non-refractory dissolved organic nitrogen by bacteria 1/day.

Refractory Dissolved Organic Nitrogen (DONre)

The refractory dissolved organic nitrogen (DONre) is produced by the degradation of the particulate organic nitrogen and decreases by mineralization to ammonia. The rate of change in refractory dissolved organic nitrogen is defined as follows:

$$\frac{\partial C^{DONre}}{\partial t} = (1-f_{orgP}) \cdot K_{dec}^{PON} \cdot C^{PON} - K_{min}^{DONre} \cdot C^{DONre} \quad [8.16]$$

Where, K^{PON}_{dec} is the rate of degradation of the particulate organic nitrogen in 1/day, K^{DONre}_{min} is the rate of mineralization of the refractory dissolved organic nitrogen in 1/day.

Phosphorus Cycle

Phosphorus cycle is demonstrated in the water quality model in basic steps of the cycle which can be summarized in the schematic figure below.

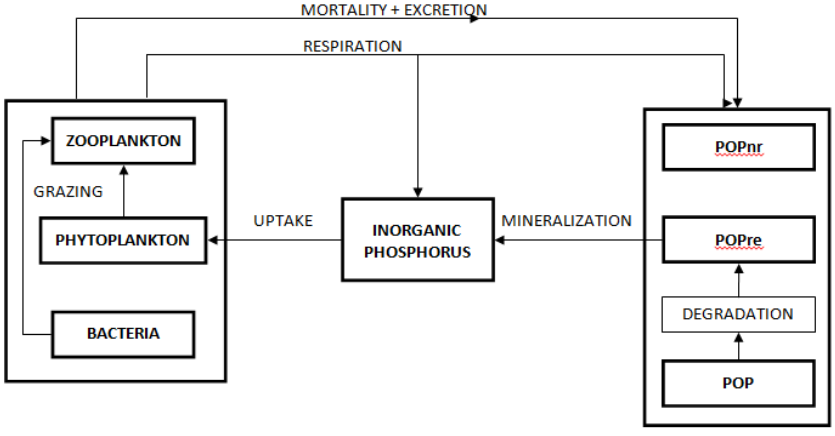

Figure 5: Phosphorus Cycle in Marine Environment

The forms of phosphorus in marine environment demonstrated in the water quality model are inorganic phosphorus (IP), particulate organic phosphorus (POP), non-refractory dissolved organic phosphorus (DOPnr), and refractory dissolved organic phosphorus (DOPre).

Inorganic Phosphorus (IP)
The sources for inorganic phosphorus are:

- Inorganic fraction of matter produced by excretion and respiration of phytoplankton,
- Inorganic fraction of matter produced by excretion and respiration of zooplankton,
- Mineralization of refractory and non-refractory dissolved organic phosphorus,
- Degradation of particulate organic phosphorus.

The rate of change in concentration of the inorganic phosphorus is formulized as follows:

$$\frac{\partial C^{IP}}{\partial t} = \begin{cases} \left[f_{in}^{f} \cdot \left(e^{f} + r^{f} \right) - \mu^{f} \right] \cdot \alpha_{P:C}^{f} \cdot C^{f} \\ + \left[f_{in}^{z} \cdot e^{z} + r^{z} \right] \cdot \alpha_{P:C}^{z} \cdot C^{z} \\ + K_{\min}^{DOPre} \cdot C^{DOPre} \\ + K_{\min}^{DOPnr} \cdot C^{DOPnr} \\ + f_{orgP} \cdot K_{dec}^{POP} \cdot C^{POP} \end{cases} \quad [8.17]$$

where, f^{f}_{in} is the inorganic fraction of matter produced by phytoplankton, f^{z}_{in} is the inorganic faction of the matter produced by zooplankton, $\alpha^{f}_{P:C}$ is the ratio of phosphorus to carbon for phytoplankton in mgP/mgC, $\alpha^{z}_{P:C}$ is the ratio of phosphorus to carbon for zooplankton in mgP/mgC, K^{DOPre}_{min} is the rate of mineralization of refractory dissolved organic phosphorus in 1/day, K^{DOPnr}_{min} is the rate of mineralization of non-refractory dissolved organic phosphorus in 1/day, K^{POP}_{dec} is the rate of degradation of particulate organic phosphorus in 1/day. The rate of mineralization of refractory dissolved organic phosphorus is formulized in the model as follows:

$$K_{\min}^{DOPre} = K_{\min}^{DOPre}(T_{ref}) \cdot \left(Q_{\min}^{DOPre} \right)^{\left(T - T_{ref}\right)} \cdot \frac{C^{f}}{K_{r}^{f} + C^{f}} \quad [8.18]$$

where, $K^{DOPre}_{min}(T_{ref})$ is the rate of mineralization of refractory dissolved organic phosphorus at reference temperature (T_{ref}) in1/day, Q_{min}^{DOPre} is the temperature coefficient for mineralization of DOPre, K^{f}_{r} is the half saturation constant for in mgC/l. The rate of mineralization of non-refractory dissolved organic phosphorus is as follows:

$$K_{\min}^{DOPnr} = K_{\min}^{DOPnr}(T_{ref}) \cdot \left(Q_{\min}^{DOPnr} \right)^{\left(T - T_{ref}\right)} \cdot \frac{C^{f}}{K_{r}^{f} + C^{f}} \quad [8.19]$$

where, $K^{DOPnr}_{min}(T_{ref})$ is the rate of the mineralization of non-refractory dissolved organic phosphorus at reference temperature (T_{ref}) in 1/day, Q_{min}^{DOPnr} is the temperature constant for mineralization of DOPnr.

The rate of degradation of the particulate organic phosphorus is formulated as follows:

$$K_{dec}^{POP} = K_{dec}^{POP}(T_{ref}) \cdot \left(Q_{dec}^{POP} \right)^{\left(T - T_{ref}\right)} \quad [8.20]$$

where, $K^{POP}_{dec}(T_{ref})$ is the rate of the degradation of particulate organic phosphorus at

reference temperature (T_{ref}) in 1/day, Q^{POP}_{dec} is the temperature coefficient for degradation of POP.

Particulate Organic Phosphorus (POP)

The sources of particulate organic phosphorus in marine environment are:

- Organic particulate fraction of the matter produced by excretion and respiration of phytoplankton,
- Mortality of phytoplankton,
- Particulate fraction of the matter that cannot be assimilated through grazing of phytoplankton and bacteria by zooplankton and the stoichiometric losses,
- Organic particulate fraction of the matter produced by excretion of zooplankton,
- Grazing and mortality of zooplankton.

POP is decreased by degradation to dissolved organic phosphorus.

The rate of change in concentration of the POP can be formulized as follows:

$$\frac{\partial C^{POP}}{\partial t} = \begin{cases} \left[\left(1-f_{in}^{f}\right)\cdot\left(1-f_{orgD}^{f}\right)\cdot\left(e^{f}+r^{f}\right)+m^{f}\right]\cdot\alpha_{P:C}^{f}\cdot C^{f} \\ +\left[\left(1-f_{in}^{z}\right)\cdot\left(1-f_{orgD}^{z}\right)\cdot e^{z}+m^{z}+p^{z}\right]\cdot\alpha_{P:C}^{z}\cdot C^{z}+\left(\delta_{P}^{z}+\varphi_{P}^{z}\right)\cdot C^{z} \\ -f_{orgP}\cdot K_{dec}^{POP}\cdot C^{POP} \end{cases} \quad [8.21]$$

where, δ^{z}_{P} is the rate production of the matter that cannot be assimilated by zooplankton during the grazing of phytoplankton and bacteria in 1/day, φ^{z}_{P} is the rate of the stoichiometric losses in 1/day, f_{orgP} is the fraction of particulate organic phosphorus available for mineralization.

The rate production of the matter that cannot be assimilated by zooplankton during the grazing of phytoplankton and bacteria is defined as:

$$\delta_{P}^{z}=\left(1-E^{f}\right)\cdot\alpha_{P:C}^{f}\cdot C_{z}^{f}+\left(1-E^{b}\right)\cdot\alpha_{P:C}^{b}\cdot C_{z}^{b} \quad [8.22]$$

where, C^{f}_{z} is the assimilation rate of phytoplankton by zooplankton in 1/day, C^{b}_{z} is the assimilation rate of bacteria by zooplankton in 1/day, E^{f} assimilation efficiency of phytoplankton by zooplankton, E^{b} is the assimilation efficiency of bacteria by zooplankton.

The rate of the stoichiometric losses for grazing of phytoplankton and bacteria by zooplankton are as follows:

$$\varphi_{P}^{z}=\left(\alpha_{P:C}^{f}-\alpha_{P:C}^{z}\right)E^{f}\cdot C_{z}^{f}+\left(\alpha_{P:C}^{b}-\alpha_{P:C}^{z}\right)E^{b}\cdot C_{z}^{b} \quad [8.23]$$

where, $\alpha^{f}_{P:C}$ is the ratio of phosphorus to carbon for phytoplankton in mgP/mgC, $\alpha^{b}_{P:C}$ is the ratio of phosphorus to carbon for pelagic bacteria in mgP/mgC, $\alpha^{z}_{P:C}$ is the ratio of phosphorus to carbon for zooplankton in mgP/mgC.

Non-refractory Dissolved Organic Phosphorus (DOPnr)

The sources of the non-refractory dissolved organic phosphorus (DONnr) are:

- The dissolved organic faction of the matter produced by excretion and respiration of the phytoplankton,
- The dissolved organic faction of the matter produced by excretion of zooplankton.

Non-refractory dissolved organic phosphorus decreases by mineralization to inorganic phosphorus. The rate of change in concentration of the non-refractory dissolved organic phosphorus (DONnr) can be formulized as follows:

$$\frac{\partial C^{DOPnr}}{\partial t} = \begin{cases} \left(1- f_{in}^{f}\right)\cdot f_{orgD}^{f}\cdot\left(e^{f}+r^{f}\right)\cdot\alpha_{P:C}^{f}\cdot C^{f} \\ +\left(1- f_{in}^{z}\right)\cdot f_{orgD}^{z}\cdot e^{z}\cdot\alpha_{P:C}^{z}\cdot C^{z} \\ -K_{\min}^{DOPnr}\cdot C^{DOPnr} \end{cases} \quad [8.24]$$

Refractory Dissolved Organic Phosphorus (DONre)

The refractory dissolved organic phosphorus increases by the degradation of the particulate organic phosphorus (POP) and decreases by mineralization to inorganic phosphorus.

The rate of change in the concentration of the refractory dissolved organic phosphorus is formulated as follows:

$$\frac{\partial C^{DOPre}}{\partial t} = (1- f_{orgP})\cdot K_{dec}^{POP}\cdot C^{POP} - K_{\min}^{DPOPre}\cdot C^{DOPre} \quad [8.25]$$

Oxygen Cycle

Oxygen cycle is demonstrated in the water quality model in basic steps of the cycle which can be summarized in the schematic figure below.

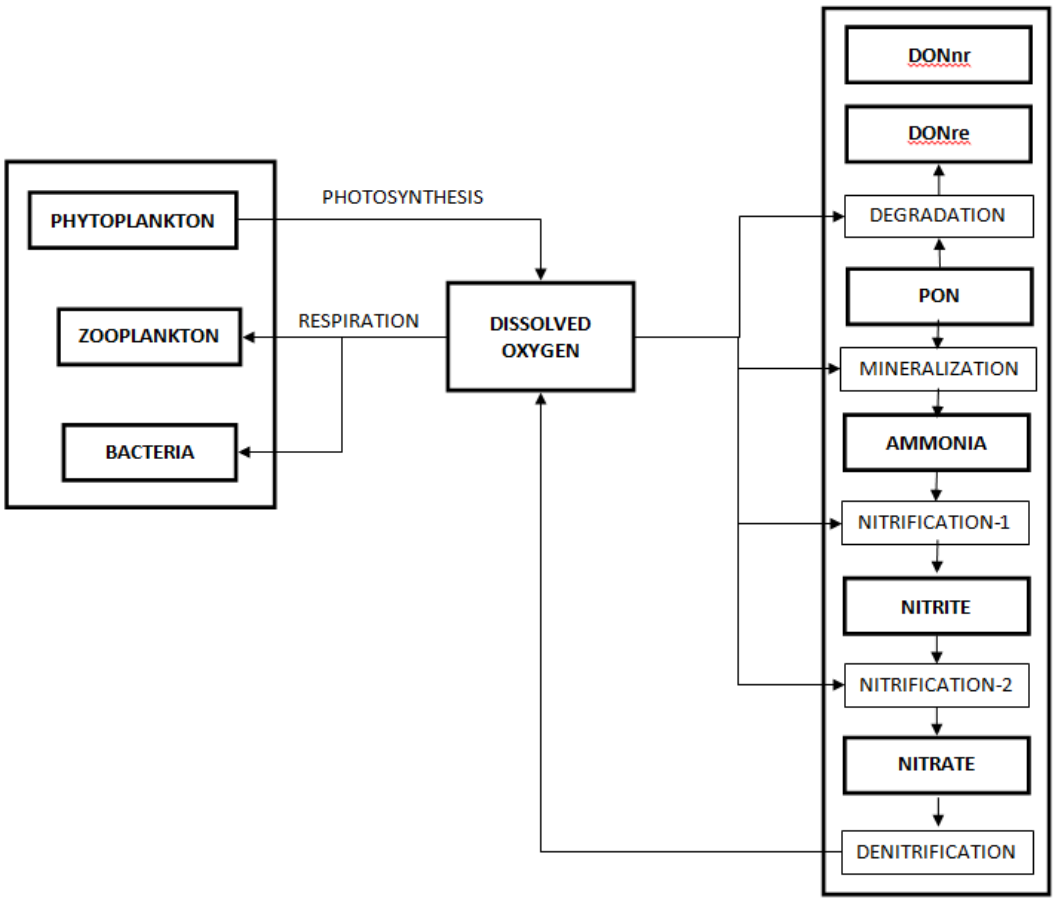

Figure 6: Oxygen Cycle in Marine Environment

Dissolved oxygen plays an important role throughout the nitrogen and phosphorus cycle as well as in the aquatic life. The sources of the dissolved oxygen in the marine environment are:

- Photosynthesis of the phytoplankton,
- Oxygen transfer across the water surface,
- Denitrification of the nitrate.

The sinks of the dissolved oxygen are:

- The respiration of the aquatic life forms,
- Degradation of the particulate organic materials,
- Mineralization of the inorganic nitrogen forms.

The rate of change in the concentration of the dissolved oxygen can be formulated as follows:

$$\frac{\partial C^{DOPre}}{\partial t} = \begin{cases} \left[\mu^f \cdot \alpha_{O:C}^{ph} + \left(1-\beta_{NH4} f\right)\cdot \mu^f \cdot \alpha_{O:N}^{NO3} \cdot \alpha_{N:C}^{f}\right]\cdot C^f \\ +\left[\mu^f \cdot \alpha_{O:P}^{IP} \cdot \alpha_{P:C}^{f} - r^f \cdot \alpha_{O:C}^{f}\right]\cdot C^f \\ -r^z \cdot \alpha_{O:C}^{z} \cdot C^z \\ -\left(\mu_{PON}^{b} + \mu_{DONnr}^{b}\right)\cdot \alpha_{O:C}^{b} \cdot C^b \\ -K_{min}^{DONre} \cdot \alpha_{O:N}^{\min} \cdot C^{DONre} \\ -K_{dec}^{POP} \cdot \alpha_{O:P}^{\min} \cdot C^{,POP} - K_{min}^{DOPre} \cdot \alpha_{O:P}^{\min} \cdot C^{DOPre} - K_{min}^{DOPnr} \cdot \alpha_{O:P}^{\min} \cdot C^{DOPnr} \\ -K_{nit}^{O} \cdot C^{NH4} + K_{dnit}^{O} \cdot C^{NO3} \end{cases} \quad [8.26]$$

Where, $\alpha^{min}_{O:N}$ oxygen consumption ratio for nitrogen mineralization in mgO/mgN/day, $\alpha^{min}_{O:P}$ oxygen consumption ratio for phosphorus mineralization in mgO/mgP/day, K^{O}_{nit} oxygen consumption rate in nitrification in 1/day, K^{O}_{dnit} oxygen consumption rate in denitrification 1/day.

The oxygen consumption rate for nitrogen mineralization can be formulated as follows:

$$\alpha_{O:N}^{\min} = \frac{1}{\alpha_{N:C}^{OM}} \cdot \alpha_{O:C}^{CO2} \cdot \frac{C^O}{0,5+C^O} \quad [8.27]$$

Similarly, the oxygen consumption ratio for phosphorus mineralization can be formulated as follows:

$$\alpha_{O:P}^{\min} = \frac{1}{\alpha_{P:C}^{OM}} \cdot \alpha_{O:C}^{CO2} \cdot \frac{C^O}{0,5+C^O} \quad [8.28]$$

Oxygen consumption rate in nitrification can be calculated as follows:

$$K_{nit}^{O} = K_{nit} \cdot \alpha_{O:N}^{NO3} \quad [8.29]$$

where, K_{nit} is the rate of nitrification in 1/day.

Oxygen consumption rate in denitrification can be calculated as follows:

$$K_{dnit}^{O} = K_{dnit} \cdot \alpha_{O:N}^{NO3} \quad [8.30]$$

where, K_{dnit} is the rate of denitrification in 1/day.

Phytoplankton

The change in the concentration of the phytoplankton is modelled as it is proposed by EPA (1985) and defined as follows:

$$\frac{\partial C^f}{\partial t} = \left[\mu^f - r^f - e^f - s^f - m^f \right] \cdot C^f - G^f \qquad [8.31]$$

where, C^f is the phytoplankton concentration in mgC/l, μ^f is the phytoplankton gross grow, r^f is the respiration rate, e^f is the excretion rate, s^f is the settling rate, m^f is the mortality rate in 1/day, G^f is the phytoplankton grazing rate in mgC/l/day.

Gross Growth Rate

The growth rate of the phytoplankton is limited by temperature, light intensity and nutrients available in the ambient water, namely phosphorus and nitrogen. The gross growth rate of the phytoplankton is described as:

$$\mu^f = \mu^f_{\max}(T_{ref}) \cdot f^f(T) \cdot f^f(L) \cdot \min[, f^f(P), f^f(N)] \qquad [8.32]$$

where, $\mu^f_{max}(T_{ref})$ is maximum gross growth rate at reference temperature in 1/day, T_{ref} is the reference temperature in ^oC, $f^f(T)$ is the growth limiting function for temperature, $f^f(L)$ is the growth limiting function for light, $f^f(N)$ is the growth limiting function for nitrogen, $f^f(P)$ is the growth limiting function for phosphorus.

The Growth Limiting Factor for Temperature

The growth limiting factor for temperature is based on the temperature-optimum curve and temperature tolerance limits of the organism, proposed by Thornton and Lessem (1978) as follows:

$$f^f(T) = K^f_A(T) \cdot K^f_B(T) \qquad [8.33]$$

where, $K_A^f(T)$ and $K_B^f(T)$ are raising limb and falling limb of the temperature curve and can be formulated as follows:

$$K^f_A(T) = \frac{K^f_1 \cdot e^{\gamma^f_1 \cdot (T - T^f_{min})}}{1 + K^f_1 \cdot \left(e^{\gamma^f_1 \cdot (T - T^f_{min})} - 1 \right)} \qquad [8.34]$$

$$K^f_B(T) = \frac{K^f_4 \cdot e^{\gamma^f_2 \cdot (T^f_{\max} - T)}}{1 + K^f_4 \cdot \left(e^{\gamma^f_2 \cdot (T^f_{\max} - T)} - 1 \right)} \qquad [8.35]$$

where, K^f_1, K^f_2, K^f_3, K^f_4 are rate multipliers for temperature limits, T^f_{min} is the minimum temperature for phytoplankton, T^f_{max} is the maximum temperature for phytoplankton in ^oC, γ^f_1, γ^f_2 are rate coefficients for temperature curve.

Rate coefficients for temperature curve γ_1^f and γ_2^f are as follows:

$$\gamma^f_1 = \frac{\ln \dfrac{K^f_2 \cdot (1 - K^f_1)}{K^f_1 (1 - K^f_2)}}{T^f_{opt.\min} - T^f_{\min}} \qquad [8.36]$$

$$\gamma^f_2 = \frac{\ln \dfrac{K^f_3 \cdot (1 - K^f_4)}{K^f_4 \cdot (1 - K^f_3)}}{T^f_{\max} - T^f_{opt.\max}} \qquad [8.37]$$

where, $T^f_{opt.min}$ is the minimum optimum temperature for phytoplankton growth and $T^f_{opt.max}$ is the maximum optimum temperature for phytoplankton growth in ºC.

The Growth Limiting Factor for Light

The relationship between the growth of phytoplankton and the ambient light intensity is formulated by using the growth limiting function for light as proposed by Steele (1965).

$$f^f(L) = \frac{I(z)}{I_{opt}} \cdot e^{\left(1-\frac{I(z)}{I_{opt}}\right)} \quad [8.38]$$

where, I_{opt} is the optimum light intensity for phytoplankton growth in W/m^2, I(z) is the light intensity at the depth z in W/m^2.

The light intensity in the ambient water is calculated according to Beer-Lambert Law as:

$$I(z) = I_o \cdot e^{-k \cdot z} \quad [8.39]$$

where, I_o is the light intensity at the water surface in W/m^2, k is the light extinction coefficient in 1/m which also varies according to the turbidity of the ambient water.

Light extinction coefficient k can be limited as a function of chlorophyll, a concentration as Parson et al. (1984) proposes:

$$k = 0,04 + 0,0088Kla + 0,054Kla^{2/3} \quad [8.40]$$

where, Kla is the chlorophyll -a concentration in µg Kla /l. In order to calculate chlorophyll-a concentration following formula can be used:

$$Kla = C_f \cdot \alpha_{Kla:C} \cdot 1000 \quad [8.41]$$

where, $\alpha_{Kla:C}$ is the chlorophyll-a to carbon rate in µg Kla /µg C.

The Growth Limiting Factor for Nitrogen

The growth limiting factor for nitrogen is based on conventional Michealis and Menten Kinetics and formulated as follows:

$$f^f(\mathrm{N}) = \frac{C^{NH4} + C^{NO3}}{K_N^f + C^{NH4} + C^{NO3}} \quad [8.5]$$

where, C^{NH4} is the concentration of ammonium in mg N/l, C^{NO3} is the concentration of nitrate in mg N/l, K^f_N is the nitrogen half-saturation constant for phytoplankton in mg N/l.

The Growth Limiting Factor for Phosphorus

The growth limiting factor for phosphorus is similar to the growth limiting factor for nitrogen.

$$f^f(P) = \frac{C^{IP}}{K_P^f + C^{IP}} \quad [8.43]$$

where, C^{IP} is the concentration of the inorganic phosphorus in mg P/l, K^f_P is the phosphorus half-saturation constant for phytoplankton in mg N/l.

Respiration Rate

Respiration rate of the phytoplankton can be described as proposed by Groden (1977) and Park et al. (1980).

$$r^f = r_e^f + r_f^f \quad [8.44]$$

where, r^f_e is the endogenous respiration rate, r^f_f is the photorespiration rate in 1/day. Endogenous and photorespiration respiration rate formulized as follows (EPA, 1985):

$$r_e^f = K_e^f \cdot e^{(0,069 \square T)} \quad [8.45]$$

$$r_f^f = K_p^f \cdot \mu^f \quad [8.46]$$

where, K^f_e is the endogenous respiration constant, K^f_p is the photorespiration constant.

Excretion Rate

Excretion rate of the phytoplankton is formulized according Collins (1980) as follows:

$$e^f = K_e \cdot \mu^f \cdot \left(1 - f(L)\right) \quad [8.47]$$

where, K_e is the fraction of photosynthesis excreted.

Mortality Rate

A modified Michealis-Menten type saturation function for phytoplankton mortality is used as proposed by Rodgers and Salisbury (1981).

$$m(T_{ref}) = m_{\max}(T_{ref}) \cdot \left(\frac{C^f / \mu^f}{K_m^f + C^f / \mu^f} \right) \quad [8.48]$$

where, K^f_m is the half-saturation rate for phytoplankton mortality in mg C/l.day.

Settling Rate

Phytoplankton settling rate is directly related with the density, size and physiologic condition of the cells, as well as the density, current velocity and the turbulence of the ambient water. Scavia (1980) has defined a modified Stoke law for the settling velocity for non-spherical shaped phytoplankton cells as follows:

$$V_s = \frac{2}{9} \cdot \frac{g \cdot R^2 \cdot (\rho_p - \rho_w)}{\nu \cdot F_s} \quad [8.49]$$

where, V_s is the settling velocity of the particle in m/day, g is the gravitational acceleration in m/day^2, R is the equivalent radius in m, ρ_p is the density of the cell in kg/m^3, ρ_w is the density of the ambient water in kg/m^3, υ is the kinematic viscosity, F_s is the shape factor.

Changes in the settling velocity can be expressed according to formula below (Tetra Tech, 1980):

$$s^f = \frac{V_s(T_{ref})}{d} \cdot f_s(T) \quad [8.50]$$

where, $V_{s,max}(T_{ref})$ is the maximum settling velocity at reference temperature in m/day, T_{ref} is the reference temperature and fs(T) is the temperature adjustment function for settling velocity. Also the temperature adjustment factor is described as follows (Tetra Tech, 1980):

$$f^s(T) = \frac{157,5}{0,069 \cdot T^2 - 5,3 \cdot T + 177,6} \quad [8.51]$$

Grazing Rate

Phytoplankton grazing is defined as a function of temperature, predator population density (i.e. zooplankton concentration), and phytoplankton concentration as proposed by EPA (1985) as follows:

$$G^f = p_z^f \cdot A_{\max}^z \cdot f_z^f(A) \cdot f^z(T) \cdot C^z \quad [8.52]$$

where, p^f_z is the phytoplankton proportion in zooplankton ingestion, A^z_{max} is the maximum ingestion rate of zooplankton in 1/day, f^f_z (A) is the limiting factor for prey concentration, f^z(T) is the limiting factor for temperature and C^z is the concentration of zooplankton in mgC/l.

Pelagic Bacteria

The rate of change in heterotrophic pelagic bacteria concentrations in the model is defined as it is proposed by Bernardes (2007).

$$\frac{\partial C^b}{\partial t} = \left[\mu^b - e^b - m^b \right] \cdot C^b - G^b \quad [8.53]$$

where, C^b is the concentration of bacteria in mgC/l, μ^b is the total bacterial uptake in 1/day, e^b is the excretion rate in 1/day, m^b is the mortality rate in 1/day, G^b is the grazing rate of the bacteria in mgC/l/day.

Total Bacterial Uptake

Total bacterial uptake is related directly to the availability of nutrients and the temperature of the ambient water and can be formulated as follows:

$$\mu^b = \mu^b_{NH4} + \mu^b_{PON} + \mu^b_{DONnr} \quad [8.54]$$

where, μ^b_{NH4} is the ammonia uptake in 1/day, μ^b_{PON} is the particulate organic nitrogen uptake in 1/day, μ^b_{DONnr} is the nonrefractory dissolved organic nitrogen uptake in 1/day.

Similar to the phytoplankton growth, bacterial uptake function can be modified by limitation factor for temperature as follows:

$$\mu^b_{NH4} = \frac{\mu^b_{\max}(T_{ref}) \cdot f^b(T) \cdot f_{NH4}^{\ b}(N)}{\alpha^b_{N:C}} \quad [8.55]$$

$$\mu^b_{PON} = \frac{\mu^b_{\max}(T_{ref}) \cdot f^b(T) \cdot f_{PON}^{\ b}(N)}{\alpha^b_{N:C}} \quad [8.56]$$

$$\mu^b_{DONnr} = \frac{\mu^b_{\max}(T_{ref}) \cdot f^b(T) \cdot f_{DONnr}^{\ b}(N)}{\alpha^b_{N:C}} \quad [8.57]$$

where, f^b_{NH4}(N), f^b_{PON}(N), f^b_{DONnr}(N) are bacterial uptake limiting functions for ammonia, particulate organic nitrogen and nonrefractory dissolved organic nitrogen, $\mu^b_{max}(T_{ref})$ is the maximum bacterial uptake in reference temperature in mgN/mgC/day, f^b(T) is the bacterial uptake limiting function for temperature according to Thornton and Lessem (1978), $\alpha^b_{N:C}$ nitrogen carbon ratio for bacteria in mgN/mgC.

Bacterial uptake limiting functions for ammonia, particulate organic nitrogen and nonrefractory dissolved organic nitrogen are defined as Michealis-Menten Half-Saturation Function as follows:

$$f_{NH4}^{b}(N)=\left\{\begin{array}{ll}\dfrac{C^{NH4}}{K_N^b+C^{NH4}} & if, C^{NH4}>C_{\min}^{b,N}\\ 0 & if, C^{NH4}\le C_{\min}^{b,N}\end{array}\right\} \quad (6)$$

$$f_{PON}^{b}(N)=\left\{\begin{array}{ll}\dfrac{C^{PON}}{K_N^b+C^{PON}} & if, C^{PON}>C_{\min}^{b,N}\\ 0 & if, C^{PON}\le C_{\min}^{b,N}\end{array}\right\} \quad (7)$$

$$f_{DONnr}^{b}(N)=\left\{\begin{array}{ll}\dfrac{C^{DONnr}}{K_N^b+C^{DONnr}} & if, C^{DONnr}>C_{\min}^{b,N}\\ 0 & if, C^{DONnr}\le C_{\min}^{b,N}\end{array}\right\} \quad (8)$$

where, K^b_N is the half saturation rate for bacterial uptake in mgN/l, $C^{b,N}_{min}$ is the minimum concentration of nutrients for bacterial uptake in mgN/l.

Grazing Rate

Grazing rate of heterotrophic pelagic bacteria is formulated similar to the grazing of phytoplankton by zooplankton as follows:

$$G^b = p_z^b \cdot A_{\max}^z \cdot f_z^b(A)\cdot f^z(T)\cdot C^z \quad (9)$$

where, p^b_z is the fraction of bacteria in zooplankton grazing.

Limiting factor for prey concentration can be defined also similar to the phytoplankton grazing.

$$f_z^b(A)=\left\{\begin{array}{ll}\dfrac{c_z^b\cdot C^b-C_z^{\min,b}}{K_A^z+(c_z^b\cdot C^b-C_z^{\min,b})} & if, (c_z^b\cdot C^b-C_z^{\min,b})>0\\ 0 & if, (c_z^b\cdot C^b-C_z^{\min,b})\le 0\end{array}\right\} \quad [8.62]$$

where, c^b_z is the assimilation efficiency of bacteria by zooplankton, $C^{min,b}_z$ is the minimum concentration of zooplankton for bacteria grazing in mgC/l, K^z_A is the half-saturation constant for bacteria grazing by zooplankton in mgC/l.

Zooplankton

The rate of change in the zooplankton concentration is defined as follows (EPA, 1985):

$$\frac{\partial C^z}{\partial t}=\left[\mu^z-r^z-m^z\right]\cdot C^z-G^z \quad [8.63]$$

where, C^z is the concentration of zooplankton in mgC/l, μ^z is the gross growth rate of zooplankton in 1/day, r^z is the respiration rate in 1/day, m^z mortality in 1/day, G^z is the grazing in mgC/l/day.

Gross Growth

Gross growth of zooplankton is defined as follows (EPA, 1985):

$$\mu^z = C_z^f\cdot E^f + C_z^b\cdot E^b \quad [8.64]$$

where, C^f_z is grazing rate of phytoplankton by zooplankton in 1/day, C^b_z is the grazing rate of bacteria by zooplankton in 1/day, E^f is the assimilation coefficient of phytoplankton by zooplankton, E^b is the assimilation coefficient of bacteria by zooplankton. Grazing rates of phytoplankton and bacteria are directly related to the concentration of zooplankton and can be formulized as follows:

$$C_z^f = \frac{G^f}{C^z} \quad [8.65]$$

$$C_z^b = \frac{G^b}{C^z} \quad [8.66]$$

Where C^z is the concentration of zooplankton, G^f and G^z are grazing rates of phytoplankton and bacteria.

Respiration Rate

Respiration rate of zooplankton is formulated as follows (EPA, 1985):

$$r^z = r^z(T_{ref}) \cdot f^z(T) \quad [8.67]$$

Where, $r^z(T_{ref})$ is the respiration rate of zooplankton at reference temperature in 1/day, $f^z(T)$ is the limiting factor for zooplankton respiration calculated similar to phytoplankton.

Mortality Rate

Mortality rate of the zooplankton is limited according to a limiting function for temperature and formulated as follows (EPA, 1985):

$$m^z = m^z(T_{ref}) \cdot f^z(T) \quad [8.68]$$

Where, $m^z(T_{ref})$ is the mortality rate of zooplankton at reference temperature in 1/day and f(T) is the mortality limiting function for temperature.

Grazing Rate

Grazing rate of zooplankton by higher trophic levels are proportional to the zooplankton concentration and formulated as follows (EPA, 1985):

$$G^z = p^z \cdot C^z \quad [8.69]$$

where, p^z is the zooplankton grazing rate in 1/day.

Conclusions

HYDROTAM 3D is a Geographic Information Systems (GIS) integrated three-dimensional baroclinic numerical model that has been developed to simulate the hydrodynamic and transport processes in coastal waters. It includes hydrodynamic, transport, turbulence, wind climate, wave climate, wave propagation, longshore sediment transport, water quality submodels. The GIS platform facilitates the time consuming task of preparation of data input and output structures. In its interface all functions of the MS Silverlight framework are available to the user in a menu driven graphical user interface (GUI). HYDROTAM 3D infrastructure is based on Cloud computing technology which is a natural evolution of the widespread adoption of telecommunication and virtualization technologies. Cloud computing describes a new supplement, consumption, and delivery model for IT services based on the Internet, and it typically involves over-the-Internet provision of HYDROTAM 3D. Therefore, HYDROTAM 3D model takes all the form of web-based tools or applications that users can access and use through a web browser as if it were a program installed locally on their own computer. In a cloud, all required HYDROTAM 3D software (operating system, database, GIS tools, business or scientific applications, etc.) reside on a service providers server external to a user's computer. Cloud computing requires less power because a lot of the processing overhead is performed at the server and not at the personal computer, so the need for an extremely powerful computers is not required and

CPU time is significantly reduced. HYDROTAM 3D Cloud computing is a platform allowing IT hardware and software runs on the Internet for various types of coastal and environmental problems (hydrotam.com).

Acknowledgement

HYDROTAM 3D project is financially supported by Scientific and Technological Research Council of Turkey (TUBİTAK) during its development. Authors would like to extend thanks to DLTM Environmental Software Technologies Limited for their financial support.

References

Balas L., İnan A, 2005. "Three dimensional modelling of turbulence", Advances in Computational Methods in Sciences and Engineering, Sayfa:48-58.

Balas, L. (2001), "Simulation of Pollutant Transport in Marmaris Bay", *Chineese Ocean Engineering Journal*, Vol.15, No.4, pp.565-578.

Balas, L. and İnan A., 2001b. Numerical modeling of mild slope equations. Proceedings of the 5th International Conference on the Mediterranean Coastal Environment, MEDCOAST 01 (Hammamet, Tunisia), 1223-1234.

Balas, L. and İnan, A., 2001a. Numerical modeling of refraction and diffraction. *Coastal Engineering V, Computer Modeling of Seas and Coastal Regions*, Southampton, UK: WIT Press, 185-194.

Balas, L. and Özhan, E. (2000), "An implicit three dimensional numerical model to simulate transport processes in coastal water bodies", *Int. Journal of Numerical Methods in Fluids*, Vol.34, 307-339.

Balas, L. and Özhan, E. (2001), "Applications of a 3-D Numerical Model to Circulations in Coastal Waters", *Coastal Engineering Journal*, Vol.43, No.2, 99-120.

Balas, L. and Özhan, E. (2002), "Three Dimensional Modelling of Stratified Coastal Waters", *Estuarine Coastal and Shelf Science*, Vol.56, 75-87.

Balas, L. and Özhan, E., 2003. A Baroclinic Three Dimensional Numerical Model Applied to Coastal Lagoons. Lecture Notes in Computer Science. Vol. 2658, 205-212.

Balas, L., 2004, Modelling of Interaction Between Surface Waves and Mud Layer, Lecture Notes in Computer Science, Vol, 3037 (618-621)

Balas, L., Cebe, K. and Akay, N., 2011, *HYDROTAM: A Coastal Engineering Model Based on Cloud Computing.* 10th International Conference on the Mediterranean Coastal Environment (MEDCOAST 2011), Rhodes, Greece.

Balas, L., İnan, A. 2010. Modeling of Induced Circulation. WSEAS Transactions on Fluid Mechanics, Vol 5, No:3, 132-143

Bernardes, B.D.L., 2007. Hydrodynamical and Ecological Modelling of the North Sea, Master Thesis, School of Engineering, Technical University of Lisbon, Portugal.

Booij, N., Holthuijsen , L.H., Ris, R.C., 1999, A third-generation wave model for coastal regions 1. Model description and validation, Journal of Geophysical Research, Vol. 104, No. C4, 7649-7666.

Booij, N., Holthuijsen, L.H., Ris, R.C., 1996, The 'SWAN' Wave Model for Shallow Water, Coastal Engineering, 668-676

Braunschweig F., Leitao P., Fernandes L., Pina P., Neves R.J.J., 2004, The object-oriented design of the integrated water modelling system MOHID, Development in Water Science, Vol 55, Part 2, 1079-1090.

Bretschneider, C. L., Forecasting Relations for Wave Generation. Look Lab/Hawaii, Cilt 1, Sayı 3. Honolulu: Department of Ocean Engineering, University of Hawaii. 1970.

Cauciono, Neves, 1999, Hydrodynamic and sediment suspension modelling in estuarine systems Part II: Application to the Western Scheldt and Gironde estuaries, Journal of Marine System, Vol 22, 117-131.

Cebe, K., Balas, L., Water Quality Modelling in Kaş Bay, Applied Mathematical Modelling, Vol:40, No:3, 1887-1913, 2016.

Cebe, K., Balas, L., Monitoring and modeling land-based marine pollution, Regional Studies in Marine Science, Vol:24, 23-39, 2018.

Collins, C.D., 1980. Formulation and Validation of a Mathematical Model of Phytoplankton Growth. Ecology. Vol. 61, pp. 639-649.

Dean, R.G. and Dalrymple, R.A., 1991. Water Wave Mechanics for Engineers and Scientists. Singapore: World Scientific Publishing Co.Pte.Ltd., 353p.

Ebersole, B.A., 1985. Refraction-Diffraction Model For Linear Water Waves. *Journal of Waterway, Port, Coastal and Ocean Engineering*, 111, pp. 939-953.

EPA, 1985. Rates, constants, and kinetics formulations in surface water quality modelling. 2nd ed. U.S. Environmental Protection Agency, Report EPA/600/3-85/040.

Foster, I., Yong Zhau, Raicu, I., and Lu, S., 2008, "Cloud Computing and Grid Computing 360-Degree Compared", *Proceedings of the Grid Computing Environments Workshop (GCE '08)*, Austin, TX (USA), November 12–16, pp.1-10.

Groden T.W., 1977. Modeling Temperature and Light Adaptation of Phytoplankton. Report No.2. Center for Ecological Modeling, Rensselaer Polytechnic Institute, Troy, New York, U.S.

Lawen J., Fieg G., Yu H., Abdel-Wahaba, A., 2012, Review of Cooling Water Discharge Simulation Models, Proceedings of the 3rd International Gas Processing Symposium, March 5 - 7 2012 ,15-22, Qatar.

Neves, R., 2007, Numerical Models as Decision Support Tools in Coastal Areas, Assessment of the Fate and Effects of Toxic Agents on Water Resources, 171–195

Nicholson, J., O'Connor, B.A., 1986, Cohesive Sediment Transort Model, Journal of Hydraulic Engineering, Vol. 112, Issue 7, 621-640.

Numanoglu Genç, A, İnan, A., Yılmaz, N., Balas, L., 2013, Modeling of Coastal Erosion in Göksu Coasts, Journal of Coastal Research, SI 65, 2155-2160

Palomar P., Lara j.L., Losada ı.J., Rodrigo M., Alvárez A., 2012 a, Near field brine discharge modelling part 1: Analysis of commercial tools, Desalination 290, 14–27

Palomar P., Lara,L.J., Losada, I.J., 2012 b, Near field brine discharge modeling part 2: Validation of commercial tools, Desalination, 290, 28–42

Parsons, T.R., Takahashi, M. and Hargrave, B., 1984. Biological Oceanographic Processes. 3rd ed., Pergamon Press, Oxford, U.K.

Rijn L.C.,, D.J.R. Walstra D.J.R., Ormondt, M., 2004, Description of TRANSPOR2004 andImplementation in Delft3D-ONLINE, Report No. Z3748.10

Ris, R.C., Holthuijsen, L..H., Booij, N., 1999, A third-generation wave model for coastal regions 2. Verification, Journal of Geophysical Research, Vol. 104, No C4, 7667-7681

Rodgers, P. and Salisbury, D., 1981. Water Quality Modeling of Lake Michigan and Consideration of the Anomalous Ice Cover of 1976-1977. Journal of Great Lakes Resources. Vol. 7(4), 467-480.

Scavia, D., 1980. An Ecological Model of Lake Ontario, Ecological Modeling. Vol. 8, 49-78.

Steele, J.H., 1965. Notes on Some Theoretical Problems in Production Ecology. In: Primary Production in Aquatic Environments. C.R. Goldman (ed.). University of California Press, Berkeley, California, U.S. 393-398.

Strowd, H.D. and Lewis, G.A. (2010), "T-Check in System-of-Systems Technologies: Cloud Computing", *Technical Note, CMU/SEI-2010-TN-009 Research, Technology, and System Solutions (RTSS) Program*, 1-58.

Teisson, C, 1991. Cohesive suspended sediment transport: feasibility and limitations of numerical modeling. J. of Hydr. Res., vol. 29, n°6, pp 755-769.

Tetra Tech, Inc. 1980. Methodology for Evaluation of Multiple Power Plant Cooling System Effects, Volume V. Methodology Application to Prototype – Cayuga Lake. Tetra Tech.

Inc., Lafayette, California. For Electric Power Research Institute. Report EPRI EA-1111.

Thornton, K.W. and Lessem, A.S., 1978. A Temperature Algorithm for Modifying B
logical Rates. Trans. Am. Fish. Soc. Vol. 107(2), 284-287.

U.S. Army Corps of Engineers, 1984, SPM, "Shore Protection Manual"

US Army Corps of Engineers, CEM, Coastal Engineering Manual, 2006. Coastal Engineering Research Center, Department of the Army, , Washington DC, USA.

Van Ledden, M., 2001, Modeling of sand and mud mixtures, Part II: A process-based sand-mud model

Wu, Y., Falconer R., Uncles, R.J., 1999, Modelling of Water Flows and Cohesive Sediment Fluxes in the Humber Estuary, UK, Marine Pollution Bulletin, Vol 37, Issues 3–7, 182–189

Yegul, U., 2005, Modeling of Suspended Sediment in Coastal Waters, MSc Thesis, Gazi University Institute Science and Technology

Yıldız I, İnan A, Balas L., 2005. "Numerical modelling of wave induced circulation", Advances in Computational Methods in Sciences and Engineering, 602-612.